Thermal characteristics of fossil fluids from the Philippine Sea slab: Insights from fluid inclusions and thermochronology

S. Sueoka[1], H. Iwano[2], T. Danhara[2], M. Niwa[1], M. Kanno[1], B.P. Kohn[3], M. Kawamura[1], T. Yokoyama[1], S. Kagami[1], Y. Ogita[1] and T. Hirata[4]

[1]Tono Geoscience Center, Japan Atomic Energy Agency, Toki 509-5102, Japan.

[2]Kyoto Fission-Track Co., Ltd., Kyoto 603-8832, Japan.

[3]School of Earth Sciences, University of Melbourne, Victoria 3010, Australia.

[4]Geochemical Research Center, Graduate School of Science, The University of Tokyo, Tokyo 113-0033, Japan.

Corresponding author: Shigeru Sueoka (sueoka.shigeru@jaea.go.jp)

Key Points:

- New approach to investigate thermal features of fossil fluid activity using geothermometry and thermochronometry
- Slab-derived fluid activity at ~150 and ~200 deg. C with no thermal anomaly associated with nearby hydrothermal veins in Southwest Japan Arc
- Fluid activity occurred either at $\geq$3-km depth and before 10 Ma or more recently but very briefly (shorter than a few months or ~10 yr)

Abstract

For quantitative understanding of thermal features of fossil fluid activity derived from the Philippine Sea slab, we applied fluid-inclusion and thermochronometric analyses to hydrothermal veins and their host rocks outcropping in the Hongu area in southwestern Japan. Although hydrothermal events at ~150°C and ~200°C were identified by fluid-inclusion analyses of quartz veins, no thermal anomaly was found associated with the veins' host rocks. Cooling ages showed no variation as a function of distance from the veins. Using zircon, we determined U–Pb ages of 77.3–66.9 Ma in the youngest population, fission-track pooled ages of 34.1–24.0 Ma, and (U–Th)/He single-grain ages of 23.6–8.7 Ma. Apatite yielded pooled fission-track ages of 12.0–9.0 Ma. All these ages can be explained by fluid flow that occurred either (1) before ~10 Ma at a depth where ambient temperature is higher than closure temperature of the apatite fission-track system (90°C–120°C, equivalent to ~3-km depth) or (2) after ~10 Ma but of such duration that is too short to have annealed fission tracks in apatite, which process requires ~10 yr at ~150°C or as short as a few months at ~200°C. Apatite fission-track ages of ~10 Ma might reflect regional mountain uplift and exhumation related to rapid subduction of the Philippine Sea slab and associated with clockwise rotation of the Southwest Japan Arc.

Plain Language Summary

In subduction zones, fluids from subducting oceanic plates influence such geological phenomena as volcanism, crustal movement, and earthquakes. In our study of thermal fluids in the Hongu area of southwestern Japan, we used a new approach to characterize the thermal features of fluids that originated from the subducting Philippine Sea plate and formed hydrothermal veins in the overlying crust. By analyzing fluid inclusions trapped in quartz crystals from the veins, we estimated the temperatures to have been ~150°C and ~200°C. We also tried measuring the degree of heating (in terms of temperature and duration) of the rocks enclosing the veins by using dating methods appropriate for the reconstruction of time–temperature histories, but the effect was too small to detect by these methods. Based on our results, we propose two possible scenarios. According to the first scenario, the fossil-fluid activity occurred so long ago (>~10 Ma) that the thermal effects were overprinted by more recent events, and the fluid–rock interaction must have occurred at >~3-km depth. The second scenario is that fossil-fluid activity was shorter than ~10 yr at ~150°C and a few months at ~200°C. Our findings contribute to further understanding of geologic phenomena in subduction zones.

1 Introduction

Subduction zones possess a globally unique set of geologic and tectonic features—combining volcanism, seismicity, and ore genesis—in which fluids derived from dehydration associated with subducting slabs play important roles (e.g., Peacock, 1990; Stern, 2002). Most of the slab-derived fluids are consumed to generate magma by lowering melting temperatures of rocks, a process that results in igneous activity along volcanic arcs (e.g., Davies and Stevenson, 1992; Grove et al., 2012) and even influences deformation along volcanic arcs by weakening the crust (e.g., Hasegawa et al., 2005). Slab-derived fluids also have been linked to non-volcanic fluid activity on the forearc side of subduction zones (Ito et al., 1983; Jarrard, 2003; Hacker, 2008; Ribeiro et al., 2013, 2015; Araya Vargas et al., 2019); such activity may also have brought hot fluids to non-volcanic areas and triggered inland seismicity (Zhao et al., 1996; Obara, 2002;

Fagereng and Diener, 2011; Kato et al., 2014) and mud-volcano eruptions (Fryer et al., 1999). Therefore, slab-derived fluids are key factors in hydrological circulation, element migration, and related geological phenomena in subduction zones. Also, understanding the properties of slab-derived fluids, such as their chemical and thermal features, is important in terms of societal and industrial demands, for example, generation of ore deposits (Cox, 2005), development of geothermal resources (Adachi et al., 2014), and safety and stability of underground facilities (National Institute of Advanced Industrial Science and Technology, 2016, 2017).

The Japanese islands in the western Pacific subduction zones, consisting of multiple island arcs (Fig. 1a). Owing to contrasts between the Southwest and Northeast Japan Arcs (subduction zones of the Philippine Sea and Pacific plates), these islands can provide suitable areas for studying slab-derived fluids. Non-volcanic slab-derived fluids have been reported in various areas along the Southwest Japan Arc, including the Kii Peninsula (Morikawa et al., 2016), the Arima region (Morikawa et al., 2005; Nishimura et al., 2006; Kusuda et al., 2014), the Miyazaki region (Ohsawa et al., 2010), and districts along the Median Tectonic Line (Amita et al., 2014), but in only limited areas along the Northeast Japan Arc, including the Iwaki area (Togo et al., 2014). The young and thin Philippine Sea slab is subducting beneath the Southwest Japan Arc at a low angle. Dehydration of this hot slab is occurring at a relatively shallow depth (~50 km) and serpentinizing the superjacent mantle, which rises by buoyancy along the slab, thereby supplying H_2O to the crust (Katayama et al., 2010; Kazahaya et al., 2014). In contrast, the old and thick Pacific slab is subducting beneath the Northeast Japan Arc at a steeper angle. Dehydration of this cold slab is occurring at a relatively deep level, (~80–100 km) while also serpentinizing the superjacent mantle, which is transported to a deeper, hotter part by mantle flow and finally releases fluids that are consumed to form mantle melt (Hasegawa et al., 2008; Katayama et al., 2010; Kazahaya et al., 2014).

These slab-derived thermal fluids in the Southwest Japan Arc, sometimes referred to as Arima-type (Sakai and Matsubaya, 1974), are characterized by particular chemical compositions. Generally enriched in NaCl, CO_2, Li, and B (Matsubaya et al., 1974; Amita et al., 2005; Nishimura et al., 2006), they also have some specific chemical properties, such as high δD, $\delta^{18}O$, and $^3He/^4He$ ratios, reflecting their origins at great depth (Matsubaya et al., 1973; Sano and Wakita, 1985; Umeda et al., 2006; Kusuda et al., 2014; Morikawa et al., 2016). Kazahaya et al. (2014) found that Arima-type fluids have (Li/Cl)>0.001 (by weight) when Cl > 200 mg/L and proposed that this characteristic can be an indicator for identifying this fluid type. However, such thermal characteristics as temperature history and the duration and spatial range of hydrothermal activity are largely unknown for Arima-type fluids; only their present temperatures at the surface are well known (Matsubaya et al., 1973).

In this study, we have attempted to estimate thermal characteristics of fossil activity of slab-derived fluids in the Hongu area on the Kii Peninsula, which is on the forearc side of the Southwest Japan Arc. Based on a combination of geothermometry and multisystem thermochronology, we used a new approach to investigate outcrops of hydrothermal veins. We measured homogenization temperatures of fluid inclusions in quartz veins to estimate temperatures of the thermal fluids that formed the veins. We also applied thermochronometric methods to the host-rock enclosing the veins to constrain the timing, duration, and spatial range of thermal-fluid activity. These methods included apatite and zircon fission-track (AFT and ZFT), zircon (U–Th)/He, and zircon U–Pb analyses. By this contribution, we have aimed to establish methods to help constrain the thermal characteristics of past hydrothermal activity from

the Philippine Sea plate. Using thermochronometry data, we also discuss the thermal and exhumation histories of the accretionary complexes in the study area.

2 Geological Setting

The Kii Peninsula is in the Outer Zone of the Southwest Japan Arc, on the forearc side of the Median Tectonic Line. The Kii Peninsula features a number of high-temperature hot springs in the Shirahama, Katsu'ura, Ryujin, Tosenji, Totsukawa, and Hongu areas, although they are a few hundred kilometers away from the volcanic front of the Southwest Japan Arc (Fig. 1b). Various studies based on geochemical and geophysical approaches support findings that the high-temperature fluids of the Kii Peninsula are derived from the Philippine Sea slab beneath the region: high geothermal gradients (Tanaka et al., 2004), $^{3}He/^{4}He$ ratios as high as 4–5 R_A (Umeda et al., 2006, 2007; Morikawa et al., 2016), high Li/Cl ratios by weight (>0.001) (Kazahaya et al., 2014), seismicity including seismic swarms (Kato et al., 2014) and deep low-frequency tremors (Obara, 2002), and low resistivity (<10 Ωm) between the Conrad discontinuity and the slab surface (Yamaguchi et al., 2009).

The Kii Peninsula is composed predominantly of the Cretaceous to Miocene accretionary complex of the Shimanto Belt and Miocene silicic rocks. The rocks of the Shimanto Belt have been roughly divided into the Cretaceous Hidakagawa, the Eocene Otonashigawa, and the Oligocene to early Miocene Muro Groups from the back-arc to forearc sides (Tokuoka et al., 1981). In the Hongu area, the Haroku Formation of the Otonashigawa Group consists mainly of alternating sandstones and mudstones (Tokuoka et al., 1981). The Haroku Formation yielded Eocene radiolarian fossils (Suzuki, 1993), and detrital zircons from the included tuffaceous sandstone produced U–Pb ages of 50.8 ± 1.0 Ma (Tokiwa et al., 2016). Also, many AFT and ZFT dates from the Shimanto Belt of the Kii Peninsula have been reported (e.g., Hasebe and Tagami, 2001; Hasebe and Watanabe, 2004; Umeda et al., 2007; Hanamuro et al., 2008; Ohira et al., 2016) that support regional exhumation and expand on local thermal histories (see Section 5.2 for further detail).

The Miocene silicic rocks have been divided into the Kumano and Omine acidic rocks, which were formed by igneous activity of the Kumano Caldera (Miura, 1999; Kawakami et al., 2007) and the Omine and Odai Cauldrons (Sato and Yamato Omine Research Group, 2006), respectively. Lithologic units of the Kumano rocks consist of both intrusive and effusive rock, including granite, granite porphyry, and pyroclastic breccia found within the accretionary complex of the Shimanto Belt (Miura, 1999). The Omine rocks are distributed in several separate masses, composed mainly of granodiorite, granite, and granite porphyry (Kawasaki, 1980). Radiometric ages for the Kumano and Omine rocks have generally been in the range ~16–14 Ma, as estimated by various methods—including AFT and ZFT (Hasebe et al., 1993a, 2000; Iwano et al., 2007, 2009), biotite K–Ar (Sumii et al., 1998; Sumii and Shinjoe, 2003), and zircon U–Pb (Orihashi et al., 2007)—suggesting that their formation and rapid post-emplacement cooling occurred in the middle Miocene.

3 Methodology

3.1 Strategies

To improve the understanding of thermal features of fossil-fluid activity derived from a slab, we suggest a new approach that combines geothermometric data from hydrothermal veins

and thermochronometric information from their host rocks (Fig. 2). Thermochronology, which can be used to constrain thermal histories of rocks and minerals on the basis of thermal resetting of radiometric ages, has been applied to many geologic processes, including mountain building, basin development, fault movement, etc. (e.g., Reiners et al., 2005; Ault et al., 2019). Cooling ages of a thermochronometer reflect thermal histories around its closure temperature: 90°C–120°C for AFT (Ketcham et al., 1999, 2007), 160°C–200°C for zircon (U–Th)/He (Reiners et al., 2004; Guenthner et al., 2013), ~300°C for ZFT (Yamada et al., 2007; Ketcham, 2019), and >900°C for zircon U–Pb systems (Cherniak and Watson, 2000) over a geologic timescale and under typical mineralogical conditions (e.g., grain morphology, chemical composition, and radiation damage). Kinetic models of thermochronometers (i.e., the relationship between cooling ages and time–temperature conditions) are described by linear or curvilinear functions in Arrhenius space wherein the ordinate axis represents logarithmic time and the abscissa axis represents reciprocal temperature (e.g., Reiners, 2009). In other words, the thermal resetting of samples depends predominantly on the duration and temperature of heating. Although in general closure temperatures of 10^6–10^7 yr are used for geologic events (e.g., Reiners et al., 2005), the duration of crustal-fluid activity is expected to be shorter. In this work we have attempted to determine paleotemperatures by using an independent geothermometer and the heating duration derived from thermochronologic data (Fig. 2).

The temperature of fossil-fluid activity is initially determined by applying geothermometry to hydrothermal-vein samples, and then the timing of the activity is estimated from cooling ages of host rocks near the veins. This strategy assumes that slab-derived fluids were hot enough to reset some of the cooling ages, depending on thermal conditions above the slab, maximum depth of the fluids, and the fluids' travel time to the shallow crust. Related more to heat conduction than to fluid migration in the host rocks, the thermal effects' spatial extent can be constrained by using multiple thermochronometric methods that have different temperature sensitivities, applied at progressive distances from the hydrothermal veins. The duration of the thermal-fluid activity can be computed by comparing the different datasets acquired from vein and host-rock samples. Because fluid temperatures are determined by geothermometry, duration of the activities also can be constrained by using kinetic models of thermometers. For example, if the cooling age of a thermochronometer is totally reset (or not reset at all), the minimal (or maximum) duration can be determined from the upper (or lower) limit of the partial retention zone. By combining multiple thermochronometers having various kinetic properties, the duration can be constrained even more precisely.

3.2 Sample collection

To follow the above strategies, we sampled hydrothermal veins and their host rocks from three locations (HJG1, HJG 2, and HJG4) in the Hongu area in the central part of the Kii Peninsula (Fig. 3). In these outcrops, alteration zones of ~0.5-m width are exposed in the sandstone and mudstone of the Haroku Formation. These zones include abundant quartz, epidote, chlorite, and sulfide minerals such as pyrite, pyrrhotite, and chalcopyrite. Widespread brown, friable deposits composed mainly of goethite fill gaps on the alteration surfaces. The vein quartz commonly shows holocrystalline, hypidiomorphic, and blocky textures, easily distinguished from the host rocks' fragmented quartz (Fig. 4). The host-rock Haroku Formation typically shows alternating beds of ~10–50-cm-thick sandstones with some interbedded ~1-cm-thick mudstones. Although these beds are often folded and have varying strikes, they mostly have gentle dips. In contrast, the near-vertical alteration zones cut the bedding of the Haroku

198 Formation, penetrating both the sandstone and mudstone. At each outcrop, one sample was
199 collected from the quartz vein for fluid-inclusion analysis, and three or four samples were
200 collected from the sandstones for thermochronometry (fission-track, (U–Th)/He, and U–Pb
201 analyses) (Table 1; Fig. 3).

202 Because intrusive rock outcrops at location HJG3 (near locations HJG1, HJG2, and
203 HJG4), a sample was obtained for U–Pb analyses, which are helpful to assess whether cooling
204 ages at locations HJG1, HJG2, and HJG4 reflect thermal effects related to the intrusion rather
205 than from thermal-fluid activity. The intrusive rock, which belongs to the Omine acidic rocks,
206 consists of coarse (φ = ~5–8 mm) quartz porphyry that contains brownish altered feldspars and
207 mafic minerals. The northern boundary between this intrusive body and the Haroku Formation is
208 sharp and strikes N57°W, 82°N.

209 ### 3.3 Analyses applied

210 Geothermometric measurements using fluid-inclusion data were performed on three
211 samples collected from the quartz veins to estimate temperatures of the geothermal activity that
212 formed the veins. Homogenization temperatures and final ice-melting temperatures were
213 measured at the Geothermal Engineering Co., Ltd. (Supp. Text S1). Geo- and thermochronologic
214 analyses via zircon (U–Th)/He, AFT and ZFT, and U–Pb zircon methods were performed on 13
215 host-rock samples. (U–Th)/He analyses were not performed on apatite because in sedimentary
216 rocks such grains commonly are rounded, and their poor morphology makes them unsuitable for
217 such analysis (e.g., Farley, 2002). Mineral separations, fission-track dating fission-track length
218 measurement, and U–Pb dating were conducted mainly at the Kyoto Fission-Track Co., Ltd.
219 (Supp. Text S2). U–Pb dating of the intrusive rock sample was done at the Tono Geoscience
220 Center, Japan Atomic Energy Agency (Supp. Text S2). Helium measurements using an
221 Alphachron system for (U–Th)/He dating were performed at the Tono Geoscience Center (Supp.
222 Text S3). U–Th content of the degassed zircons was measured at the University of Melbourne
223 (Supp. Text S3).

224 ## 4 Analytical Results

225 ### 4.1 Fluid-inclusion analyses

226 Results of the fluid-inclusion analyses (Table 2) show that their occurrence in the
227 samples was generally poor owing mainly to low transparent of the fluid-inclusions.
228 Homogenization temperatures were estimated to be 140°C–145°C (n =3) for sample HJG1-F and
229 110°C–216°C (n =10) for HJG2-F. By measuring only primary inclusions, reproducible results
230 were obtained for each of these two samples, ranging within 144°C–145°C for HJG1-F and
231 195°C–211°C for HJG2-F. We interpreted these temperatures as reflecting fluid temperatures at
232 the time of formation of the quartz veins. (No data were obtained from HJG4-F owing to a lack
233 of two-phase fluid inclusions.) The wide range of homogenization temperatures obtained from
234 secondary inclusions in HJG2-F may indicate diverse fluid activity at various temperatures after
235 initial vein formation. Final ice-melting temperatures were difficult to measure owing to the
236 small size of the fluid inclusions. Only six measurements (including from secondary inclusions)
237 were obtained from HJG2-F, yielding final ice-melting temperatures of −5.0°C–−0.4°C and salt
238 concentrations of 0.7 wt%–7.9 wt%.

On the basis of fluid-inclusion microthermometry performed on quartz and calcite veins obtained from two boreholes in the Hongu area, Oishi et al. (1995) identified at least three past hydrothermal episodes with characteristics as follows: (1) high temperatures (250°C–350°C) and mineralization of quartz, calcite, and pyrrhotite; (2) intermediate temperatures (150°C–250°C) and mineralization of pyrite, quartz, and calcite; and (3) low temperatures (80°C–150°C). Considering the estimated fluid temperatures and the mineral compositions, the veins that we studied are thought to have formed during the second of these three hydrothermal episodes. This agreement with our data suggests that our homogenization temperatures are accurate.

4.2 U–Pb analyses

Among the U–Pb dating results for the host-rock samples (Supp. Figs. S1–S3), the grain ages generally infer populations dated at ~75 Ma, ~90 Ma, ~200 Ma, and/or ~1.7 Ga (Supp. Fig. S1). In this study, we adopted the youngest of these populations for inter-sample comparison. For each sample, we calculated a weighted mean ^{238}U–^{206}Pb age from concordant age grains whose ages overlap within ±3σ of the youngest grain age, yielding computed ages ranging from 77.3 ± 1.5 Ma to 66.9 ± 1.9 Ma (Supp. Figs. S1 and S2).

Among the U–Pb dating results from Omine acidic rocks (Supp. Fig. S3), sample HJG3-UPb produced eight discordant ages from 25 measurements (Supp. Figs. S3a and S3b), which probably are related to common Pb contamination from tiny inclusions. Therefore, we instead used the weighted mean obtained from the 17 concordant ^{238}U–^{206}Pb ages, 14.87 ± 0.57 Ma (±2σ) (Supp. Fig. S3c). As a secondary standard, OD-3 zircons were simultaneously measured, yielding the concordia age of 32.6 ± 0.94 Ma (±1σ) (Fig. S3d) with Iwano et al.'s (2013) reference age 33.0 ± 0.1 Ma (±2σ), thereby supporting accuracy of our dating results.

4.3 Fission-track analyses

We obtained pooled FT ages ranging 34.1 ± 1.4 to 24.0 ± 1.1 Ma from zircon and 12.0 ± 1.2 to 9.0 ± 1.0 Ma from apatite (Table 3). Zircon grains with ^{238}U–^{206}Pb ages of ~75 Ma and ~90 Ma have comparable ZFT ages in the range of ~100–10 Ma (Supp. Fig. S2). However, zircons with ^{238}U–^{206}Pb ages of ~200 Ma and ~1.7 Ga tend to yield more dispersed ages, ranging within ~180–10 Ma. Considering the bimodal distributions of the fission-track length data (Supp. Fig. S4), these ages apparently reflect partial annealing by reheating; accordingly, we assume that the shorter confined tracks (<~8 μm) were formed prior to the reheating event, and the longer ones (~11 μm) were formed after the event. The difference in age dispersion is thought to be from differences in fission-track ages prior to the reheating event. However, given the low fission-track densities (Table 3), relatively few apatite track lengths were measured for each sample (Supp. Fig. S5). Although ^{252}Cf-irradiation was performed on the apatite in an effort to increase confined tracks (Donelick and Miller, 1991), large etch pits obscured identification and measurement of the confined tracks.

4.4 (U–Th)/He analyses

We performed zircon (U–Th)/He dating of unknown grains from HJG1 and HJG2 samples and simultaneously analyzed Fish Canyon Tuff reference zircons (Table 4). The tuff generally produced widely dispersed ages, including two grains (016 and 017) that yielded extraordinarily low eU values, resulting in anomalously older ages, probably indicating incomplete digestion of the zircons before U–Th measurements. Grain 015 also appears to be

anomalously old, but with a higher eU value, possibly owing to U–Th zonation (Hourigan et al., 2005). Except for those three grains, the weighted mean age of 27.7 ± 3.1 Ma is consistent with the reference value, 28.3 ± 0.4 Ma (Gleadow et al., 2015), implying accuracy of dating results for our unknowns. Relative error of the weighted mean age of Fish Canyon Tuff zircons (1σ = ~11.2%) was adopted as a total uncertainty of our (U-Th)/He analytical procedures, being applied to error of grain ages of the unknowns (Table 4). Grain ages of the unknowns are in the range 23.6–8.7 Ma, except for two outliers (HJG2-10m-006 and HJG1-20m-010). HJG2-10m-006 might be monazite considering the extremely high U and Th content. HJG1-20m-010 may be digested incompletely because it yielded the lowest Th contents. The weighted mean age of the other grains, 16.8 ± 3.9 Ma, is consistent with the ZFT and AFT ages, taking into account their different ranges of closure temperatures.

5 Geological Implications

5.1 Tectonothermal scenarios and thermal features of fossil-fluid activity

From the spatial patterns of the thermochronometric data plotted against distance from quartz veins in the alteration zones (Fig. 5), we observed no significant variation in any system or parameter, even in the AFT system, which has the lowest closure temperature of the systems shown. Thermal effects from the quartz porphyry dike of the Omine acidic rocks at location HJG3 are negligible because cooling ages determined from samples obtained at locations HJG1, HJG2, and HJG4 are neither coeval with the zircon U–Pb age based on samples taken at location HJG3 nor in agreement with formation and cooling at ~16–14 Ma, as established for the Omine acidic rocks (Hasebe et al., 2000; Sumii and Shinjoe, 2003; Iwano et al., 2007, 2009). Accordingly, the dating results could be explained by reheating related to fluid-flow activity and/or regional thermal and exhumation histories rather than to dike intrusion. Three possible tectonothermal scenarios are discussed as follows.

In the first scenario, only the AFT system was totally reset for all the outcrops by fluid activity at ~10 Ma, whereas the other systems were not affected. However, this scenario is the least likely of the three because such thermal histories and structures are difficult to reproduce. For complete annealing of AFTs over all the outcrops, higher temperatures and/or longer heating periods would have been required and would have resulted in some resetting of the other thermochronometers, at least in the vicinity of the veins. Thus, the AFT ages of ~10 Ma might be interpreted as reflecting regional cooling and exhumation rather than local reheating by fluid activity. Also, other thermochronometric system data are most likely related to regional events, at least in the study area.

The second and third scenarios interpret the AFT ages as reflecting regional cooling and exhumation, with differences in timing of fluid activity: before ~10 Ma in the second scenario and after ~10 Ma in the third scenario (Fig. 6). In the second scenario, thermal effects on the AFT ages by fluids prior to ~10 Ma were overprinted by the later cooling and exhumation (Fig. 6a). Such activity must have occurred at a depth where the ambient temperature was higher than the AFT system closure temperature, generally ~90°C–120°C for apatites with low Cl content (e.g., Ketcham et al., 1999) although it is fundamentally difficult to constrain thermal features of the fluid activity based on the AFT data. This would equate to a depth of >~3 km if a general thermal gradient of 20°C–30°C/km is assumed. Based on the difference between fluid temperatures estimated from fluid-inclusion analyses and ambient temperature, any increase in

temperatures associated with hydrothermal fluids is constrained to not exceed the range 20°C–130°C.

In the third scenario, fluid activity postdates the ~10-Ma regional cooling and exhumation but had no effect on the AFT system (Fig. 6b). In this scenario, the duration of fluid activity can be constrained by using annealing functions of the AFT system. The r = 0.93 line in Fig. 7 denotes the typical time–temperature conditions under which fission tracks start to anneal. Considering the fossil-fluid temperatures of ~150°C and ~200°C estimated from fluid-inclusion analyses, the duration needs to be shorter than ~10 yr at the lower temperature or a few months at the higher temperature to preclude annealing of the tracks. These estimates are consistent with characteristic durations for pulses of slab-fluid release, which have been estimated to be from a few months to 10^2 yr on the basis of Li-isotope analysis and Li-diffusion modeling of hydrothermal veins (John et al., 2012; Taetz et al., 2018; Beinlich et al., 2020). This agreement indicates the effectiveness of our new approach. However, these durations are shorter than expected because major slab-derived hot springs in the Southwest Japan Arc, such as Arima, Dogo, Shirahama, and Hongu, have been recorded in many historical records since before 1000 yr ago. If this scenario applies, then fluid flow may have frequently switched paths locally over a network of paths in existence for at least a millennium.

It is difficult to determine which is more likely between the second and third scenarios on the sole basis of data obtained in this study. Age estimates for the formation of the hydrothermal veins could help because the timing of the fluid flow is different for the two scenarios. Direct dating of quartz cannot be done, but one possible solution would be to apply the methodologies used here to other regions where slab-derived-fluid activity has been established. Verification in more slowly cooled and exhumed regions would be especially desirable because undisturbed host rocks in such regions would yield older cooling ages, which are easier to distinguish from cooling ages reflecting recent hydrothermal-fluid activity. Nonetheless, our results point to a possible new approach that could be used to estimate and constrain some thermal features of fossil-fluid systems.

5.2 Regional thermal and exhumation history of accretionary complexes

Regional thermal and exhumation history of the accretionary complexes in the study area was also constrained by using the thermochronologic data. The data of all 13 samples were integrated (Fig. 8) because they were collected within a range of <1 km (Fig. 3) and therefore were expected to have a common thermal history with no local thermal disturbances. Using integrated fission-track ages and apatite and zircon fission-track-length data, we applied thermal inversion using HeFTy v.1.9.3 software (Ketcham, 2005) (Supp. Text S4).

ZFT and AFT thermochronology has been used to investigate the thermal and exhumation history of the accretionary complexes of the Shimanto Belt on the Kii Peninsula (e.g., Tagami et al., 1995; Hasebe and Tagami, 2001; Hasebe and Watanabe, 2004) as well as in other regions in the Southwest Japan Arc (Hasebe et al., 1993b, 1997) (Fig. 9). In the eastern part of Shikoku Island, the maximum temperature during accretion varies regionally. Cretaceous rocks of the Northern Shimanto Belt were heated to the ZFT partial annealing zone (PAZ), yielding younger grain ages than the age of deposition. However, grains in rocks of the Southern Shimanto Belt are older than their Eocene–Miocene time of deposition, so they have not been heated to the ZFT PAZ (Hasebe et al., 1993b; Tagami et al., 1995). In contrast, AFT ages of ~10 Ma were obtained in both the Northern and Southern Shimanto Belts. These AFT ages are

significantly younger than the deposition ages, reflecting a rapid cooling and exhumation episode straddling the AFT PAZ at ~10 Ma (Hasebe et al., 1993b). Fission-track data in western Shikoku Island and Kyushu Island indicate similar thermal histories, except for local reheating episodes, such as the granitic intrusion at ~15 Ma (Tagami and Shimada, 1996; Hasebe et al., 1997; Hasebe and Tagami, 2001). Fission-track data for the Kii Peninsula are also largely consistent with other regions but differ in the following points: (1) AFT ages young southward from ~35 Ma to ~13 Ma in the Northern Shimanto Belt and are ~6 Ma in the Southern Shimanto Belt (Hasebe and Tagami, 2001); (2) young AFT ages (~5–2.5 Ma) near hot springs have been reported (Umeda et al., 2007; Hanamuro et al., 2008); (3) a patchy distribution of Miocene ZFT ages probably related to heat influx has been observed (Hasebe and Watanabe, 2004); and (4) accretion-related heating to the upper limit of the ZFT PAZ has been determined for some regions of the Northern Shimanto Belt (Ohira et al., 2016).

In this study, we found that ZFT lengths have a bimodal distribution, generally implying a reheating episode or long residence time within the ZFT PAZ (with subsequent cooling below the ZFT PAZ), and ZFT grain ages that are generally younger than the Eocene depositional age (Figs. 8b and 8c). Considering that ZFT ages of ~80–70 Ma were reported in adjacent areas in the Southern Shimanto Belt (Umeda et al., 2007; Hanamuro et al., 2008), the younger ZFT ages in this study may have been partially reset by a reheating episode related to heat influx (Hasebe and Watanabe, 2004). AFT ages of ~10 Ma in this study are consistent with the southward younging trend, considering that the study area is in the northern part of the Southern Shimanto Belt. AFT lengths show a unimodal, negatively skewed distribution (Fig. 8a), which is typical of undisturbed bedrock (cf. Gleadow et al., 1986), indicating relatively slow cooling through the AFT PAZ. Although thermal inversion results prior to ~20 Ma are not considered to be meaningful, results calculated for two scenarios commonly indicate residence in the ZFT PAZ prior to ~15 Ma, subsequent rapid cooling at ~15–10 Ma through to the AFT PAZ, and slightly slower cooling from ~10 Ma to the present surface temperature (Figs. 8d and 8e). The cooling history since ~15 Ma is interpreted as reflecting regional exhumation of the accretionary complexes, likely associated with mountain development of the Outer Zone of the Southwest Japan Arc, i.e., the Kii, Shikoku, and Kyushu mountains. Together with AFT ages previously determined for the Kii Peninsula (Hasebe and Tagami, 2001), Shikoku (Hasebe et al., 1993b, 1997) and Kyushu (Hasebe and Tagami, 2001), these mountains are thought to have been uplifted and exhumed at ~10 Ma although only the Kii Mountains were tilted northward. These mountains were uplifted mainly at ~15–10 Ma and then their exhumation slowed; in contrast, most other mountains on the islands of Japan were uplifted mainly under east–west compression since the late Pliocene (e.g., Yonekura et al., 2001). The mountains in the Outer Zone might have been uplifted by a very different mechanism, such as by rapid subduction (>10 cm/yr) of the Philippine Sea plate during the clockwise rotation of the Southwest Japan Arc at the end of the opening of the Sea of Japan (Kimura et al., 2005).

6 Conclusions

We applied fluid-inclusion analyses and thermochronometry for understanding thermal features of fossil slab-derived hydrothermal activity in the Hongu area on the forearc side of the Southwest Japan Arc. Temperatures of fluids at the time of forming of the veins are estimated to have been ~150°C and ~200°C. However, the zircon U–Pb ages 77.3–66.9 Ma, ZFT ages 34.1–24.0 Ma, zircon (U–Th)/He ages of 23.6–8.7 Ma, and AFT ages of 12.0–9.0 Ma show no spatial variation with distance from the veins. These results could be explained by the following two

scenarios: (1) fluid activity prior to ~10 Ma at >90°C–120°C, or (2) fluid activity after ~10 Ma and over a timespan <10 yr at ~150°C or a few months at ~200°C. In the first scenario, the elevation in temperature is constrained at less than 20°C–130°C. These results suggest that our new approach, based on geothermometry and thermochronometry, is useful to estimate and constrain thermal features of fossil-fluid activity, although further verification would be desirable. AFT ages of ~10 Ma may reflect mountain uplift and exhumation in the Outer Zone of Southwest Japan Arc, possibly triggered by rapid slab subduction during clockwise rotation of the Southwest Japan Arc.

Acknowledgments, Samples, and Data

This study was funded by the Ministry of Economy, Trade and Industry (METI), Japan as part of its R&D supporting program titled “Establishment of Advanced Technology for Evaluating the Long-term Geosphere Stability on Geological Disposal Project of Radioactive Waste (Fiscal Years 2018 and 2019)”. We appreciate valuable comments by Prof. Takahiro Tagami (Kyoto University). Fluid inclusion analyses were carried out by Geothermal Engineering Co., Ltd. We thank Kiyotaka Yoshikawa (JAEA) for supporting the sample preparation. Field trip and sample collection were supported by Tsuneari Ishimaru, Akiomi Shimada, Koji Shimada, Tetsuya Komatsu, Hiroki Amamiya, Tadamasa Ueki, Terumasa Tozawa, Daiki Ogawa (JAEA) and Messrs. Ura and Tani (Hongu branch office of Tanabe city office). Some figures are drawn by using the Generic Mapping Tools (GMT; Wessel and Smith, 1991), 50-m mesh DEM and GSI Map of the Geospatial Information Authority of Japan (GSI), and the GEBCO_08 Grid of the General Bathymetric Chart of the Oceans (GEBCO). The University of Melbourne thermochronology laboratory receives support under the AuScope program of the National Collaborative Research Infrastructure Strategy (NCRIS). The data for this paper are presented in the tables and supporting information, whereas data archiving is underway via PANGAEA (https://www.pangaea.de/); the data to be archived (seven files) are provided as Supporting Information for review purposes.

References

Adachi, M., Ariki, K., Goto, H., Saeki, K., & Morita, S. (2014), A conceptual model for controls of geothermal reservoirs, *Journal of Hot Spring Sciences*, 63, 364–381 (in Japanese with English abstract).

Amita, K., Ohsawa, S., Du, J., & Yamada, M. (2005), Origin of Arima-type deep thermal water from hot spring wells in Oita plain, eastern Kyushu, Japan, *Journal of Hot Spring Sciences*, 55, 64–77 (in Japanese with English abstract).

Amita, K., Ohsawa, S., Nishimura, K., Yamada, M., Mishima, T., Kazahaya, K., Morikawa, N., & Hirajima, T. (2014), Origin of saline waters distributed along the Median Tectonic Line in southwest Japan: Hydrogeochemical investigation on possibility of derivation of metamorphic dehydrated fluid from subducting oceanic plate, *Journal of Japanese Association of Hydrological Sciences*, 44, 17–38 (in Japanese with English abstract).

Araya Vargas, J., Meqbel, N. M., Ritter, O., Brasse, H., Weckmann, U., Yanez, G., & Godoy, B. (2019), Fluid distribution in the Central Andes subduction zone imaged with magnetotellurics, *Journal of Geophysical Research: Solid Earth*, 124, 4017–4034.

Ault, A. K., Gautheron, C., & King, G. E. (2019), Innovations in (U–Th)/He, fission track, and trapped charge thermochronometry with applications to earthquakes, weathering, surface-mantle connections, and the growth and decay of mountains, Tectonics, 38, https://doi.org/10.1029/2018TC005312.

Beinlich, A., John, T., Vrijmoed, J. C., Tominaga, M., Magna, T., & Podladchikov, Y. Y. (2020), Instantaneous rock transformations in the deep crust driven by reactive fluid flow, *Nature Geoscience*, 13, 307–311.

Carlson, W. D., Donelick, R. A., & Ketcham, R. A. (1999), Variability of apatite fission-track annealing kinetics: I. Experimental results, *American Mineralogist*, 84, 1213–1223.

Cherniak, D. J., & Watson, E. B. (2000), Pb diffusion in zircon, *Chemical Geology*, 172, 5–24.

Committee for Catalog of Quaternary Volcanoes in Japan (1999), Catalog of Quaternary Volcanoes in Japan v1.0, CD-ROM Version, Volcanological Society of Japan.

Cox, S. F. (2005), Coupling between deformation, fluid pressures, and fluid flow in ore-producing hydrothermal systems at depth in the crust, *Economic Geology 100th Anniversary Volume*, pp.39–75.

Davies, J. H., & Stevenson, D. J. (1992), Physical model of source region of subduction zone volcanics, *Journal of Geophysical Research*. 97, 2037–2070.

Donelick, R. A, & Miller, D. S. (1991), Enhanced TINT fission track densities in low spontaneous track density apatite using ^{252}Cf-derived fission fragment tracks: A model and experimental observations, *Nuclear Tracks and Radiation Measurements*, 18, 301–307.

Fagereng, Å., & Diener, J. F. A. (2011), Non-volcanic tremor and discontinuous slab dehydration, *Geophysical Research Letters*, 38, L15302, doi:10.1029/2011GL048214.

Farley, K. A. (2002), (U–Th)/He dating: Techniques, calibrations, and applications, *Reviews in Mineralogy & Geochemistry*, 47, 819–844.

Farley, K. A., Wolf, R. A., & Silver, L. T. (1996), The effects of long alpha-stopping distances on (U-Th)/He ages, *Geochimica et Cosmochimica Acta*, 60, 4223–4229.

Fryer, P., Wheat, C. G., & Mottl, M. J. (1999), Mariana blueschist mud volcanism: Implications for conditions within the subduction zone, *Geology*, 27, 103–106.

Galbraith, R. F. (1990), The radial plot: graphical assessment of spread in ages, *International Journal of Radiation Applications and Instrumentation. Part D. Nuclear Tracks and Radiation Measurements*, 17, 207–214.

Gleadow, A. J. W., Duddy, I. R., Green, P. F., & Lovering, J. F. (1986), Confined fission track lengths in apatite: a diagnostic tool for thermal history analysis, *Contributions to Mineralogy and Petrology*, 94, 405–415.

Gleadow, A. J. W., Harrison, M., Kohn, B., Lugo-Zazueta, R., & Phillips, D. (2015), The Fish Canyon Tuff: Anew look at an old low-temperature thermochronology standard, *Earth and Planetary Science Letters*, 424, 95–108.

Grove, T. L., Till, C. B., & Krawczynski, M. J. (2012), The role of H_2O in subduction zone magmatism, *Annual Review of Earth and Planetary Sciences*, 40, 413–439.

Guenthner, W. R., Reiners, P. W., Ketcham, R. A., Nasdala, L., & Giester, G. (2013), Helium diffusion in natural zircon: Radiation damage, anisotropy, and the interpretation of zircon (U-Th)/He thermochronology, *American Journal of Science*, 313, 145–198.

Hacker, B. R. (2008), H_2O subduction beyond arcs, *Geochemistry, Geophysics, Geosystems*, 9, Q03001. doi:10.1029/2007GC001707.

Hanamuro, T., Umeda, K., Takashima, I., & Negishi, Y. (2008), Thermal history of the alteration zones around hot springs at Hongu and Totsukawa area, Southern Kii Peninsula, Southwest Japan, *Japanese Magazine of Mineralogical and Petrological Sciences*, 37, 27–38 (in Japanese with English abstract).

Hasebe, N., Suwargadi, B. W., & Nishimura, S. (2000), Fission track ages of the Omine Acidic Rocks, Kii Peninsula, Southwest Japan, *Geochemical Journal*, 34, 229–235.

Hasebe, N., Tagami, T., & Nishimura, S. (1993a), The evidence of along-arc differential uplift of the Shimanto accretionary complex: Fission track thermochronology of the Kumano Acidic Rocks, Southwest Japan, *Tectonophysics*, 224, 327–335.

Hasebe, N., Tagami, T., & Nishimura, S. (1993b), Evolution of the Shimanto accretionary complex: A fission-track thermochronologic study, *Geological Society of America Special Paper*, 273, 121–136.

Hasebe, N., Tagami, T., & Nishimura, S. (1994), Towards zircon fission-track thermochronology: Reference framework for confined track length measurements, *Chemical Geology (Isotope Geoscience Section)*, 112, 169–178.

Hasebe, N., Tagami, T., & Nishimura, S. (1997), Melange-forming processes in the development of an accretionary prism: Evidence from fission track thermochronology, *Journal of Geophysical Research*, 102, 7659–7672.

Hasebe, N., & Tagami, T. (2001), Exhumation of an accretionary prism: results from fission track thermochronology of the Shimanto Belt, southwest Japan, *Tectonophysics*, 331, 247–267.

Hasebe, N., & Watanabe, H. (2004), Heat influx and exhumation of the Shimanto accretionary complex: Miocene fission track ages from the Kii Peninsula, southwest Japan, *Island Arc*, 13, 533–543.

Hasegawa, A., Nakajima, J., Umino, N., & Miura, S. (2005), Deep structure of the northeastern Japan arc and its implications for crustal deformation and shallow seismic activity, *Tectonophysics*, 403, 59–75.

Hasegawa, A., Nakajima, J., Kita, S., Tsuji, Y., Nii, K., Okada, T., Matsuzawa, T., & Zhao, D. (2008), Transportation of H_2O in the NE Japan subduction zone as Inferred from seismic observations: supply of H_2O from the slab to the arc crust, *Journal of Geography*, 117, 59–75 (in Japanese with English abstract).

Hirose, F., Nakajima, J., & Hasegawa, A. (2008a), Three-dimensional seismic velocity structure and configuration of the Philippine Sea slab in southwestern Japan estimated by double-difference tomography, *Journal of Geophysical Research*, 113, B09315, doi:10.1029/2007JB005274.

Hirose, F., Nakajima, J., & Hasegawa, A. (2008b), Three-dimensional velocity sructure and configuration of the Philippine Sea slab beneath Kanto district, central Japan, estimated by

534 double-difference tomography, *Zisin (Journal of the Seismological Society of Japan. 2nd ser.)*,
535 60, 123-138 (in Japanese with English abstract).

536 Hourigan, J. K., Reiners, P. W., & Brandon, M. T. (2005), U-Th zonation dependent alpha-
537 ejection in (U-Th)/He chronometry, *Geochimica et Cosmochimica Acta*, 69, 3349–3365.

538 Ito, E., Harris, D. M., & Anderson Jr., A. T. (1983), Alteration of oceanic crust and geologic
539 cycling of chlorine and water, *Geochimica et Cosmochimica Acta*, 47, 1613–1624.

540 Iwano, H., Danhara, T., Hoshi, H., Kawakami, Y., Sumii, T., Shinjoe, H., & Wada, Y. (2007),
541 Simultaneity and similarity of the Muro Pyroclastic Flow Deposit and the Kumano Acidic Rocks
542 in Kii Peninsula, southwest Japan, based on fission track ages and morphological characteristics
543 of zircon, *Journal of Geological Society of Japan*, 113, 326–339 (in Japanese with English
544 abstract).

545 Iwano, H., Danhara, T., & Hoshi, H. (2009), Fission track ages on apatite from Miocene igneous
546 rocks in the Kii Peninsula, Japan, *Journal of Geological Society of Japan*, 115, 427–432 (in
547 Japanese with English abstract).

548 Iwano, H., Orihashi, Y., Hirata, T., Ogasawara, M., Danhara, T., Horie, K., Hasebe, N., Sueoka,
549 S., Tamura, A., Hayasaka, Y., Katsube, A., Ito, H., Tani, K., Kimura, J., Chang, Q., Kouchi, Y.,
550 Haruta, Y., & Yamamoto, K. (2013), An inter-laboratory evaluation of OD-3 zircon for use as a
551 secondary U–Pb dating standard, *Island Arc*, 22, 382–394.

552 Jarrard, R. D. (2003), Subduction fluxes of water, carbon dioxide, chlorine, and potassium,
553 *Geochemistry, Geophysics, Geosystems*, 4, 8905, http://dx.doi.org/10.1029/2002GC000392.

554 John, T., Gussone, N., Podladchikov, Y. Y., Bebout, G. E., Dohmen, R., Halama, R., Klemd, R.,
555 Magna, T., & Seits, H.-M. (2012), Volcanic arcs fed by rapid pulsed fluid flow through
556 subducting slabs, *Nature Geoscience*, 5, doi:10.1038/ngeo1482.

557 Katayama, I., Hirauchi, K., & Nakajima, J. (2010), Variability of subduction processes beneath
558 Japan, *Journal of Geography*, 119, 205–223 (in Japanese with English abstract).

559 Kato, A., Saiga, A., Takeda, T., Iwasaki, T., & Matsuzawa, T. (2014), Non-volcanic seismic
560 swarm and fluid transportation driven by subduction of the Philippine Sea slab beneath the Kii
561 Peninsula, Japan, *Earth, Planets and Space*, 66, 86, http://www.earth-planets-
562 space.com/content/66/1/86.

563 Kawakami, Y., Hoshi, H., & Yamaguchi, Y. (2007), Mechanism of caldera collapse and
564 resurgence: Observations from the northern part of the Kumano Acidic Rocks, Kii peninsula,
565 southwest Japan, *Journal of Volcanology and Geothermal Research*, 167, 263–281.

566 Kawasaki, M. (1980), Omine Acid Rocks, Kii Peninsula: Geology and major element chemistry,
567 *Journal of the Japanese Association of Mineralogists, Petrologists and Economic Geologists*, 75,
568 86–102.

569 Kazahaya, K., Takahashi, M., Yasuhara, M., Nishio, Y., Inamura, A., Morikawa, N., Sato, T.,
570 Takahashi, H. A., Kitaoka, K., Ohsawa, S., Oyama, Y., Ohwada, M., Tsukamoto, H., Horiguchi,
571 K., Tosaki, Y., & Kirita, T. (2014), Spatial distribution and feature of slab-related deep-seated
572 fluid in SW Japan, *Journal of Japanese Association of Hydrological Sciences*, 44, 3–16 (in
573 Japanese with English abstract).

574 Ketcham, R. A. (2005), Forward and inverse modeling of low-temperature thermochronometry
575 data, *Reviews in Mineralogy & Geochemistry*, 58, 275–314.

576 Ketcham, R. A. (2019), Fission-track annealing: From geologic observations to thermal history
577 modeling, In Malusà, M. G., & Fitzgerald, P. G. (eds.) Fission-Track Thermochronology and its
578 Application to Geology, Springer Textbooks in Earth Sciences, Geography and Environment,
579 pp.49–75.

580 Ketcham, R. A., Carter, A., Donelick, R. A., Barbarand, J., & Hurford, A. J. (2007), Improved
581 modeling of fission-track annealing in apatite, *American Mineralogist*, 92, 799–810.

582 Ketcham, R. A., Donelick, R. A., & Carlson, W. D. (1999), Variability of apatite fission-track
583 annealing kinetics: III. Extrapolation to geological time scales, *American Mineralogist*, 84,
584 1235–1255.

585 Kimbara, K. (2005), Distribution Map and Catalogue of Hot and Mineral Springs in Japan
586 (Second Edition) (CD-ROM Version), Geological Survey of Japan, AIST, Tsukuba.

587 Kimura, J., Stern, R. J., & Yoshida, T. (2005), Reinitiation of subduction and magmatic
588 responses in SW Japan during Neogene time, *Geological Society of America Bulletin*, 117, 969–
589 986.

590 Kusuda, C., Iwamori, H., Nakamura, H., Kazahaya, K., & Morikawa, N. (2014), Arima hot
591 spring waters as a deep-seated brine from subducting slab, *Earth, Planets and Space*, 66, 119.

592 Matsubaya, O., Sakai, H., Kusachi, I., & Satake, H. (1973) Hydrogen and oxygen isotopic ratios
593 and major element chemistry of Japanese thermal water systems, *Geochemical Journal*, 7, 123–
594 151.

595 Matsubaya, O., Sakai, H., & Tsurumaki, M. (1974), Hydrogen and oxygen isotropic ratios of
596 thermal and mineral springs in Arima area, *Papers of the Institute for Thermal Spring Research,*
597 *Okayama University*, 43, 15–28 (in Japanese with English abstract).

598 Miura, D. (1999), Arcuate pyroclastic conduits, ring faults, and coherent floor at Kumano
599 caldera, southwest Honshu, Japan, *Journal of Volcanology and Geothermal Research*, 92, 271–
600 294.

601 Morikawa, N., Kazahaya, K., Yasuhara, M., Inamura, A., Nagao, K., Sumino, H., & Ohwada, M.
602 (2005), Estimation of groundwater residence time in a geologically active region by coupling
603 ^{4}He concentration with helium isotope ratios, *Geophysical Research Letters*, 32, L02406,
604 doi:10.1029/2004GL021501.

605 Morikawa, N., Kazahaya, K., Takahashi, M., Inamura, Takahashi, H., Yasuhara, M., Ohwada,
606 M., Sato, T., Nakama, A., Handa, H., Sumino, H., & Nagao, K. (2016), Widespread distribution
607 of ascending fluids transporting mantle helium in the fore-arc region and their upwelling
608 processes: Noble gas and major element composition of deep groundwater in the Kii Peninsula,
609 southwest Japan, *Geochemica et Cosmochimica Acta*, 182, 173–196.

610 Nakajima J., & Hasegawa, A. (2007), Subduction of the Philippine Sea plate beneath
611 southwestern Japan: Slab geometry and its relationship to arc magmatism, *Journal of*
612 *Geophysical Research*, 112, B08306, doi:10.1029/2006JB004770.

Nakajima J., Hirose, F., & Hasegawa, A. (2009), Seismotectonics beneath the Tokyo metropolitan area, Japan: Effect of slab-slab contact and overlap on seismicity, *Journal of Geophysical Research*, 114, B08309, doi:10.1029/2008JB006101.

Nakata, T., & Imaizumi, T. (2002), Digital Active Fault Map of Japan, University of Tokyo Press, Tokyo, (in Japanese with English Abstract).

National Institute of Advanced Industrial Science and Technology (2016), https://www.nsr.go.jp/data/000186554.pdf (in Japanese).

National Institute of Advanced Industrial Science and Technology (2017), https://www.nsr.go.jp/data/000210763.pdf (in Japanese).

Nishimura, S., Katsura, I., & Nishida, J. (2006), Geological structure of Arima hot-spring, *Journal of Hot Spring Sciences*, 56, 3–15 (in Japanese with English abstract).

Obara, K. (2002), Nonvolcanic deep tremor associated with subduction in southwest Japan, *Science*, 296, 1679–1681.

Ohira, H., Kasai, M., Yamamoto, D., & Takasu, A. (2016), Fission track ages from accretionary complexes of Cretaceous Shimanto Belt in the Kii Peninsula, SW Japan, *Geoscience Reports of Shimane University*, 34, 69–75 (in Japanese with English abstract).

Ohsawa, S., Amia, K., Yamada, M., Mishima, T., & Kazahaya, K. (2010), Geochemical features and genetic process of hot-spring waters discharged from deep hot-spring wells in the Miyazaki plain, Kyushu Island, Japan: Diagenetic dehydrated fluid as a source fluid of hot-spring water, *Journal of Hot Spring Sciences*, 59, 295–309 (in Japanese with English abstract).

Oishi, A., Muramatsu, Y., Yoshida, Y., & Hashizume, R. (1995), Hydrothermal activity in Hongu area, Wakayama Pref., based on the fluid inclusion geothermometry, *Journal of Hot Spring Sciences*, 45, 63–75 (in Japanese with English abstract).

Orihashi, Y., Iwano, H., Hirata, T., Danhara, T., & Shinjoe, H. (2007), U–Pb ages and trace element compositions of reddish, colorless, and detrital zircons in the Kumano Acidic Rocks in the Outer Zone of southwest Japan and origin of the host magma, *Journal of Geological Society of Japan*, 113, 366–383 (in Japanese with English abstract).

Peacock, S. M. (1990), Fluid processes in subduction zones, *Science*, 248, 329–337.

Reiners, P. W. (2009), Nonmonotonic thermal histories and contrasting kinetics of multiple thermochronometers, *Geochimica et Cosmochimica Acta*, 73, 3612–3629.

Reiners, P. W., Ehlers, T. A., & Zeitler, P. K. (2005), Past, present, and future of thermochronology, *Reviews in Mineralogy & Geochemistry*, 58, 1–18.

Reiners, P. W., Spell, T. L., Nicolescu, S., & Zanetti, K. A., (2004), Zircon (U-Th)/He thermochronometry: He diffusion and comparisons with 40Ar/39Ar dating, *Geochimica et Cosmochimica Acta*, 68, 1857–1887.

Ribeiro, J. M., Stern, R. J., Kelley, K. A., Martinez, F., Ishizuka, O., Manton, W. I., & Ohara, Y. (2013), Nature and distribution of slab-derived fluids and mantle sources beneath the Southeast Mariana forearc rift, *Geochemistry, Geophysics, Geosystems*, 14, 4585–4607.

Ribeiro, J. M., Stern, R. J., Kelley, K. A., Shaw, A. M., Martinez, F., & Ohara, Y. (2015), Composition of the slab-derived fluids released beneath the Mariana forearc: Evidence for shallow dehydration of the subducting plate, *Earth and Planetary Science Letters*, 418, 136–148.

Roedder, E. (1984), *Fluid Inclusions*. Chantilly, VA: Mineralogical Society of America.

Sakai, H., & Matsubaya, O. (1974), Isotopic geochemistry of the thermal waters of Japan and its bearing on the Kuroko Ore solutions, *Economic Geology*, 69, 974–991.

Sano, Y., & Wakita, H. (1985), Geophysical distribution of $^{3}He/^{4}He$ ratios in Japan: implications for arc tectonics and incipient magmatism, *Journal of Geophysical Research*, 90, 8729–8741.

Sato, T., & Yamato Omine Research Group (2006), Omine and Odai Cauldrons: Arcuate and semicircular faults, dike swarms and collapse structure in the central area of the Kii Mountains, Southwest Japan, *Earth Science (Chikyu Kagaku)*, 60, 403–413 (in Japanese with English abstract).

Shuster, D. L., Flowers, R. M., & Farley, K. A. (2006), The influence of natural radiation damage on helium diffusion kinetics in apatite, *Earth and Planetary Science Letters*, 249, 148–161.

Stern, R. J. (2002), Subduction zones, *Reviews of Geophysics*, 40, 1012, http://dx.doi.org/10.1029/2001RG000108 (2002).

Sueoka, S., & Tagami, T. (2019), Low-temperature thermochronological database of bedrock in the Japanese Islands, *Island Arc*, e12305, https://doi.org/10.1111/iar.12305.

Sumii, T., & Shinjoe, H. (2003), K–Ar ages of the Ohmine Granitic Rocks, south-west Japan, *Island Arc*, 12, 335–347.

Sumii, T., Uchiumi, S., Shinjoe, H., & Shimoda, G. (1998), Re-examination on K-Ar age of the Kumano Acidic Rocks in Kii Peninsula, Southwest Japan, *Journal of Geological Society of Japan*, 104, 387–394 (in Japanese with English abstract).

Suzuki, H. (1993), Discovery of Eocene radiolaria from the Otonashigawa Belt of the Shimanto Superbelt in the Kii Peninsula, Southwest Japan, *Earth Science (Chikyu Kagaku)*, 47, 75–79 (in Japanese with English abstract).

Taetz, S., John, T., Brocker, M., Spandler, C., & Stracke, A. (2018), Fast intraslab fluid-flow events linked to pulses of high pore fluid pressure at the subducted plate interface, *Earth and Planetary Science Letters*, 482, 33–43.

Tagami, T., Hasebe, N., & Shimada, C. (1995), Episodic exhumation of accretionary complexes: Fission-track thermochronologic evidence from the Shimanto Belt and its vicinities, southwest Japan, *Island Arc*, 4, 209–230.

Tagami, T., & Shimada, C. (1996), Natural long-term annealing of the zircon fission track system around a granitic pluton, *Journal of Geophysical Research*, 101, 8245–8255.

Tanaka, A., Yamano, M., Yano, Y., & Sasada, M. (2004), Geothermal Gradient and Heat Flow Data in and around Japan, Digital Geoscience Map DGM P-5, Geological Survey of Japan, Tsukuba.

Togo, Y. S., Kazahaya, K., Tosaki, Y., Morikawa, N., Matsuzaki, H., Takahashi, M., Sato, T. (2014), Groundwater, possibly originated from subducted sediments, in Joban and Hamadori

areas, southern Tohoku, Japan, *Earth, Planets and Space*, 66, 131, http://www.earth-planets-space.com/content/66/1/131.

Tokiwa, T., Takeuchi, M., Shimura, Y., Ota, A., & Yamamoto, K. (2016), U–Pb ages of detrital zircon from the tuffaceous sandstone of the Shimanto Belt in the Kii Peninsula. *Journal of Geological Society of Japan*, 122, 625–635 (in Japanese with English abstract).

Tokuoka, T., Harata, T., Inouchi, Y., Ishigami, T., Kimura, K., Kumon, F., Nakajo, K., Nakaya, S., Sakamoto, T., Suzuki, H., & Taniguchi, J. (1981), Geology of the Ryujin district. Quadrangle Series, scale 1:50,000, 69p, Geological Survey of Japan, Tsukuba (in Japanese with English abstract).

Umeda, K., Hanamuro, T., Yamada, K., Negishi, Y., Iwano, H., & Danhara, T. (2007), Thermochronology of non-volcanic hydrothermal activity in the Kii Peninsula, Southwest Japan: Evidence from fission track dating and helium isotopes in paleo-hydrothermal fluids, *Radiation Measurements*, 42, 1647–1654.

Umeda, K., Ogawa, Y., Asamori, K., & Negi, T. (2006), Aqueous fluids derived from a subducting slab: Observed high ^{3}He emanation and conductive anomaly in a non-volcanic region, Kii Peninsula southwest Japan, *Journal of Volcanology and Geothermal Research*, 149, 47–61.

Vermeesch, P. (2009), RadialPlotter: A Java application for fission track, luminescence and other radial plots, *Radiation Measurements*, 44, 409–410.

Wakita, K., Igawa, T., & Takarada, S. (2009), Seamless geological map of Japan at a scale of 1:200,000 DVD edition, Digital Geoscience Map DGM G-16, Geological Society of Japan, AIST, Tsukuba.

Wessel, P., & Smith, W. H. F. (1991), Free software helps map and display data, *Eos, Transactions, American Geophysical Union*, 72, 441.

Yamada, R., Murakami, M., & Tagami, T. (2007), Statistical modelling of annealing kinetics of fission tracks in zircon; Reassessment of laboratory experiments, *Chemical Geology*, 236, 75–91.

Yamada, R., Tagami, T., & Nishimura, S. (1995), Confined fission-track length measurement of zircon: assessment of factors affecting the paleotemperature estimate, *Chemical Geology (Isotope Geoscience Section)*, 119, 293–306.

Yamaguchi, S., Uyeshima, M., Murakami, H., Sutoh, S., Tanigawa, D., Ogawa, T., Oshiman, N., Yoshimura, R., Aizawa, K., Shiozaki, I., & Kasaya, T. (2009), Modification of the Network-MT method and its first application in imaging the deep conductivity structure beneath the Kii Peninsula, southwestern Japan, *Earth Planets, and Space*, 61, 957–971.

Yonekura, N., Kaizuka, S., Nogami, M., & Chinzei, K. (eds.) (2001), Regional Geomorphology of the Japanese Islands, vol. 1, Introduction to Japanese Geomorphology, University of Tokyo Press, Tokyo, 349p (in Japanese).

Zhao, D., Kanamori, H., Negishi, H., & Wiens, D. (1996), Tomography of the source area of the 1995 Kobe earthquake: Evidence for fluids at the hypocenter? *Science*, 274, 1891–1894.

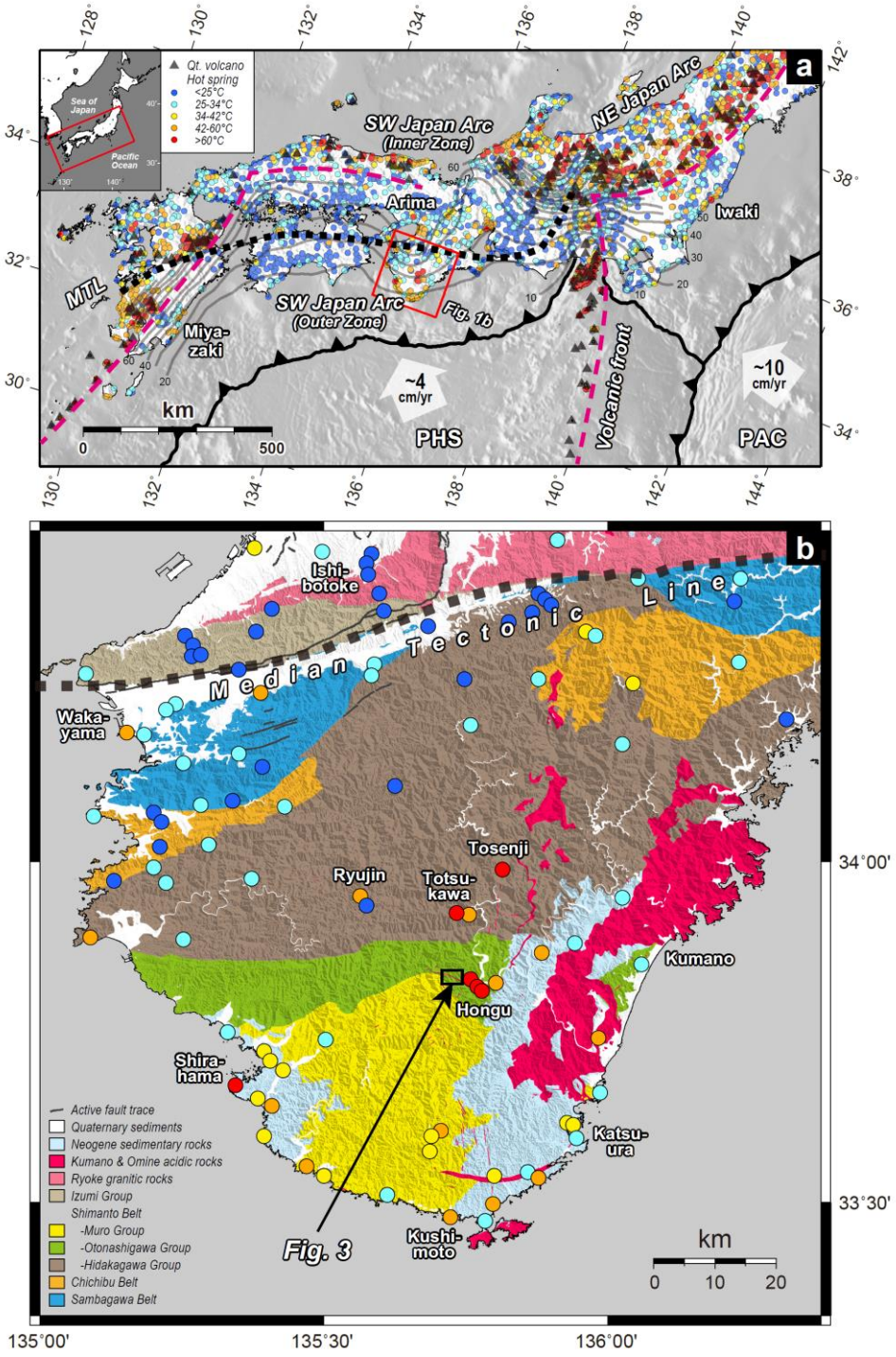

729

730 **Figure 1**. Map of study area. (a) Tectonic and hydrologic settings of Southwest Japan Arc. Data
731 for quaternary volcanoes and hot springs are from Committee for Catalog of Quaternary
732 Volcanoes in Japan (1999) and Kimbara (2005), respectively. Gray contours denote depth of
733 upper surface of PHS slab at 10-km intervals (Nakajima and Hasegawa, 2007; Hirose et al.,
734 2008a, b; Nakajima et al., 2009); (b) Geologic map of Kii Peninsula, modified after Wakita et al.
735 (2009), showing active fault traces (Nakata and Imaizumi, 2002). [MTL, Median Tectonic Line;
736 NE, Northeast; PAC, Pacific plate; PHS, Philippine Sea plate; SW, Southwest]

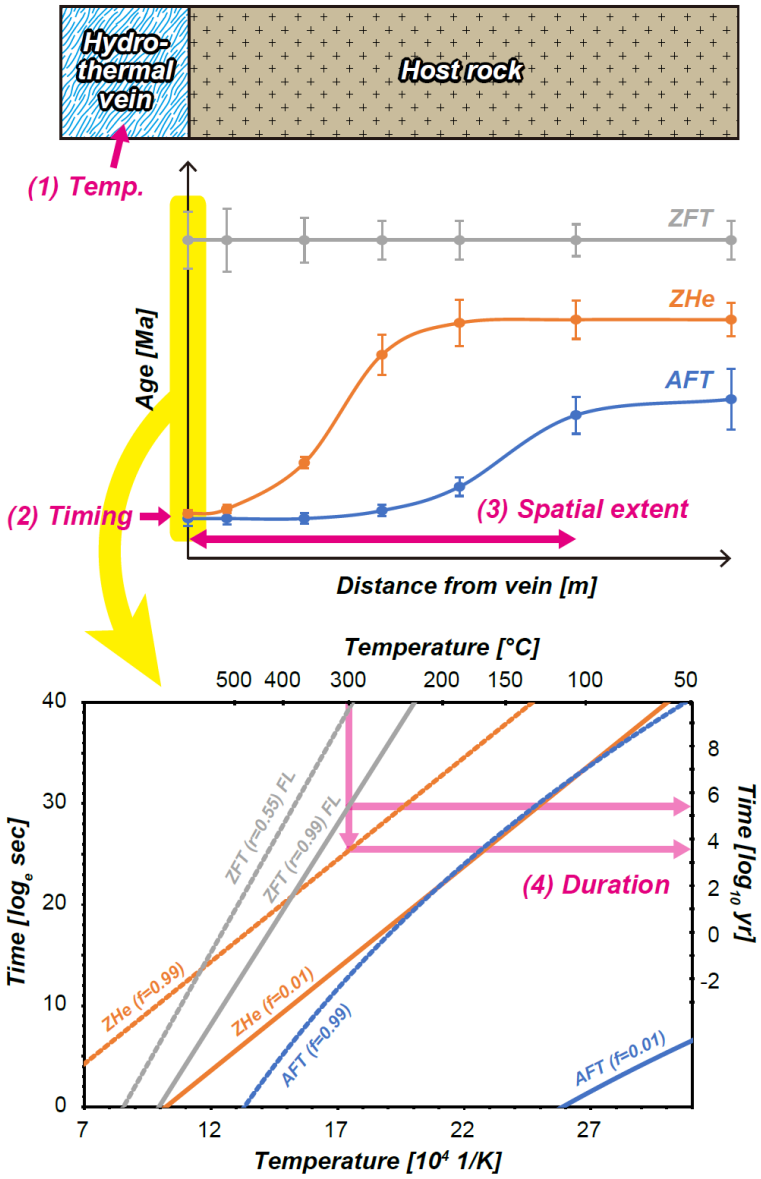

Figure 2. Schematic plots showing basic concepts of sampling and analytical strategies. (1) Temperature of fluids is estimated from hydrothermal veins by using geothermometers. (2) Dates of fluid activity can be equal to cooling ages of host rocks nearest to veins if ages are totally reset by heating. (3) Spatial pattern of thermal effects of fluid activity is constrained from thermochronometric data obtained from host rocks at various distances from veins. Regional cooling and exhumation histories are reconstructed from undisturbed host rocks at some distance from veins. (4) Duration of fluid activity can be constrained by comparing thermochronometric data from host rocks nearest to veins. If a thermochronometric system is reset and another is not, heating duration can be constrained by kinetics of those systems and temperatures estimated in (1). Plots denote fractional-loss contours of ZFT, ZHe, and AFT systems constructed after Yamada et al. (2007) and Reiners (2009), respectively. [AFT, apatite fission track; f, fractional loss; FL, Fanning linear model; *r*, reduced fission-track lengths; ZFT, zircon fission track; ZHe, zircon (U–Th)/He]

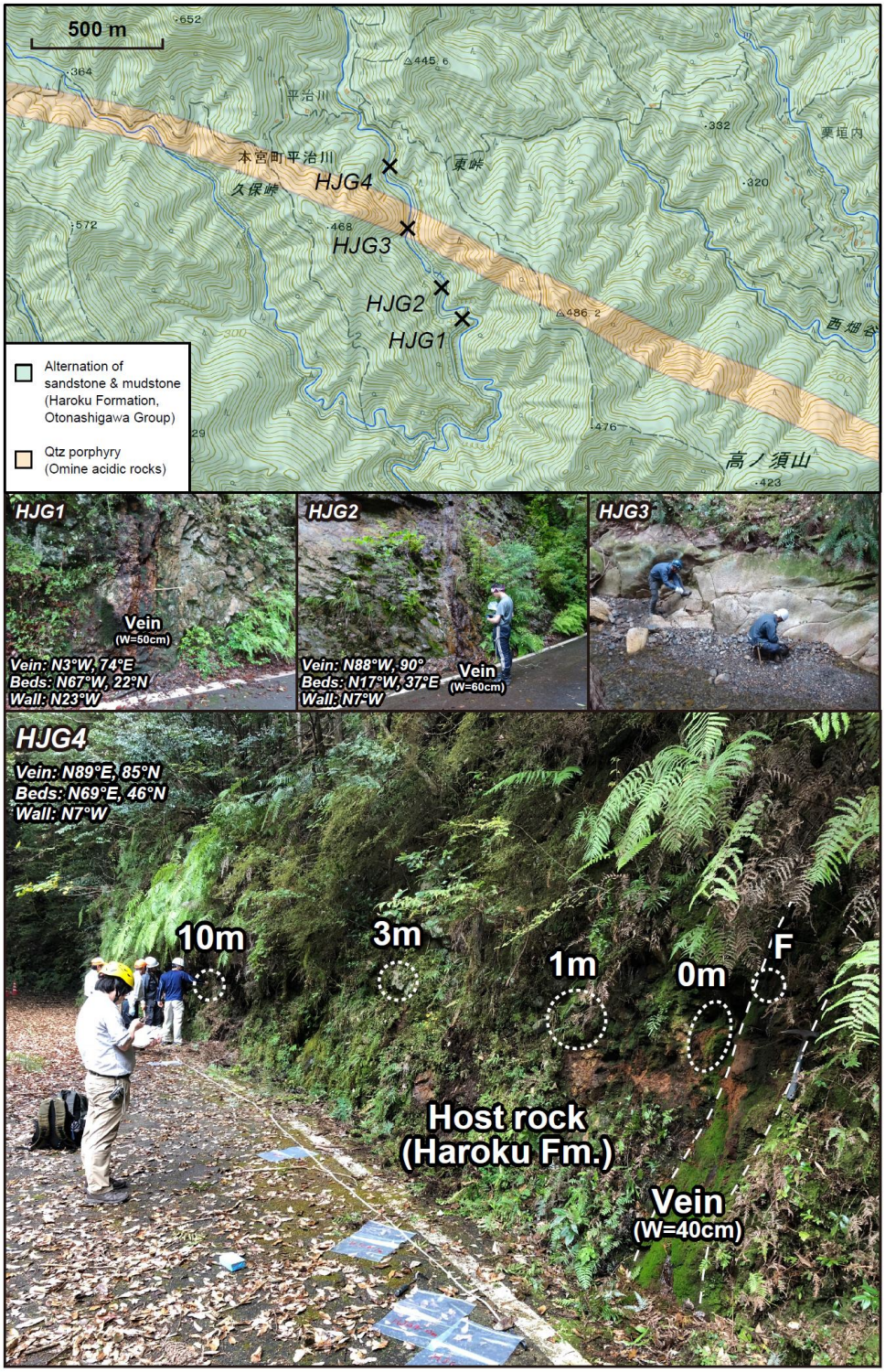

Figure 3. Sample localities and outcrop photos. Map based on Wakita et al.'s (2009) geologic map and on GSI Maps from Geospatial Information Authority of Japan. Strikes incorporate declination correction of ~7°W. Field photos show veins and specific sampling locations (HJG1, HJG2, HJG3, and HJG4). Dashed circles or ellipses in HJG4 photo show specific sample sites of HJG4-F, -0m, -1m, -3m, and -10m. [Fm., Formation; Qtz, quartz; W, width]

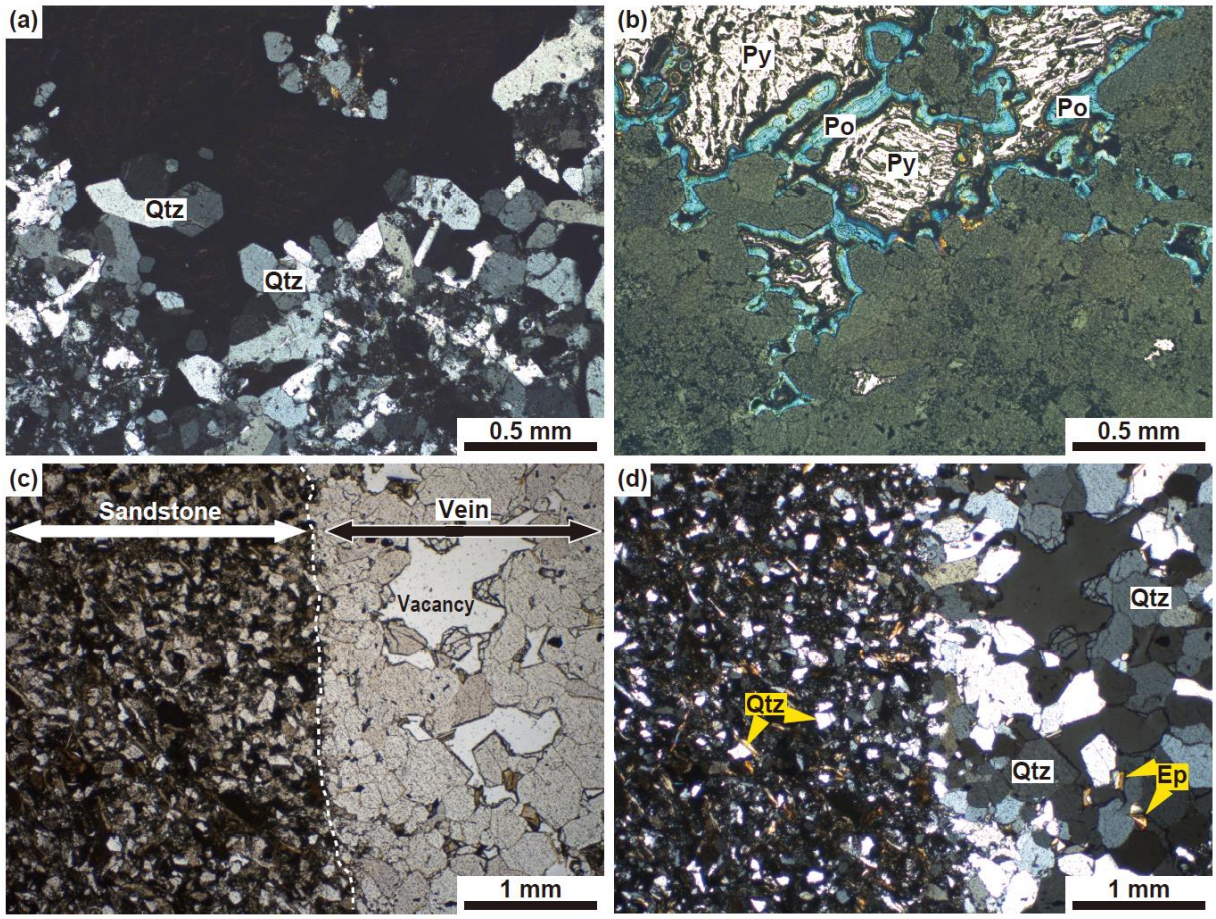

Figure 4. Photomicrographs of vein rocks from alteration zone in HJG1. (a, b) Quartz in blocky-textured vein rock under cross-polarized and reflected light; (c, d) Veins cutting through sandstone, under plane-polarized and cross-polarized light; quartz in vein is holocrystalline and hypidiomorphic but in sandstone is fragmented. [Ep, epidote; Po, pyrrhotite; Py, pyrite; Qtz, quartz]

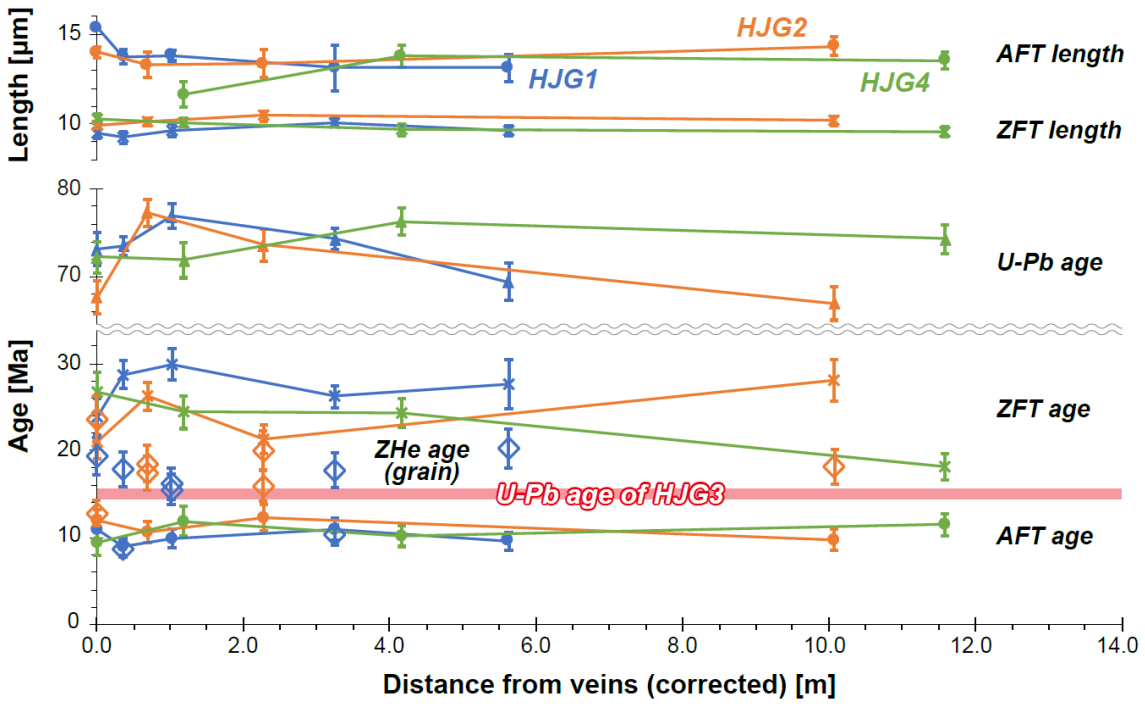

764

765 **Figure 5**. Thermochronometric data plotted against distance from veins. Distances are calibrated
766 against strike and dip of veins. Error bars for data are ±1 standard error for fission-track lengths,
767 ±1σ for fission-track ages, and ±2σ for U–Pb ages. Zircon (U–Th)/He are provided in grain ages
768 ±1σ without lines connecting the markers. [AFT, apatite fission-track; ZFT, zircon fission-track;
769 ZHe, zircon (U–Th)/He]
770

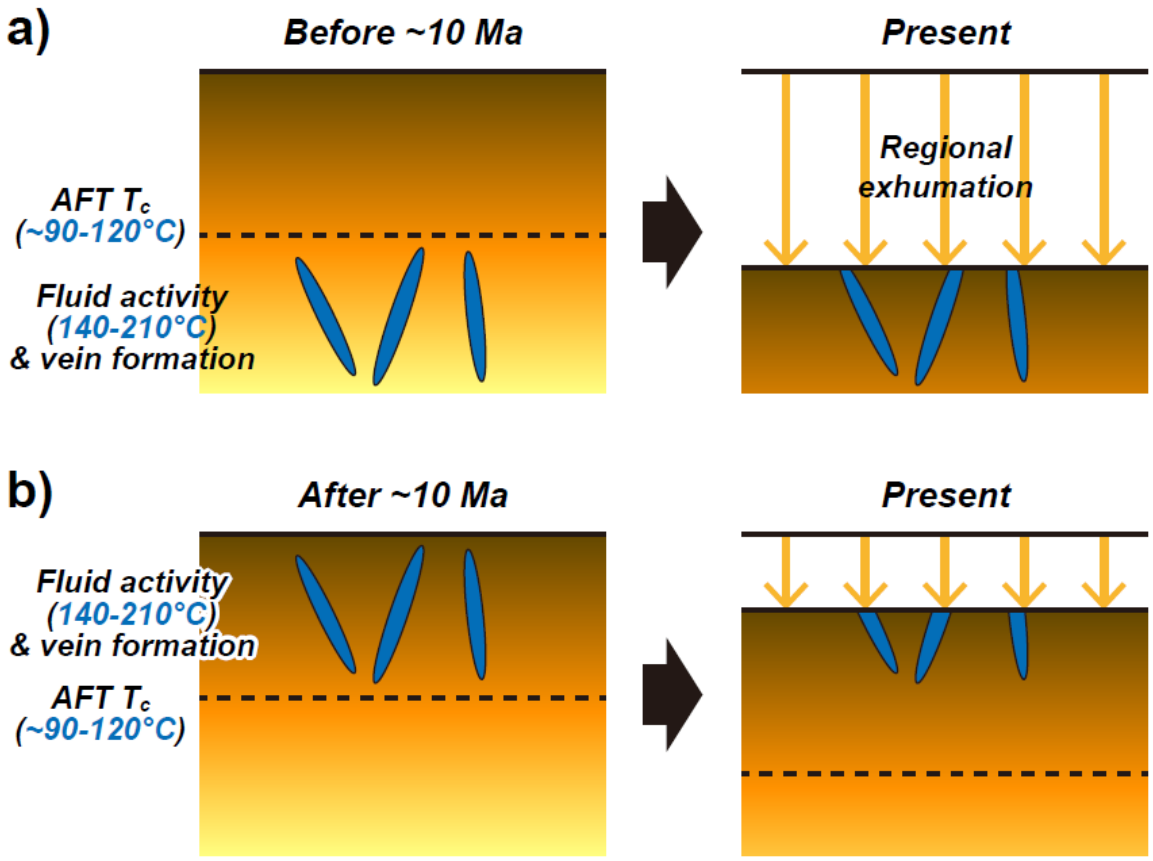

Figure 6. Sketches of possible thermal history scenarios. (a) AFT ages reflect regional exhumation at ~10 Ma with fluid activity occurring earlier than ~10 Ma; rise in temperature associated with fluid activity can be calculated from ambient and fluid temperatures; (b) AFT ages reflect regional exhumation at ~10 Ma and fluid activity that has occurred later than ~10 Ma. Fluid activity had no effect on ages because of its short duration, which can be constrained by annealing functions of AFT system (see Fig. 7). [AFT, apatite fission-track]

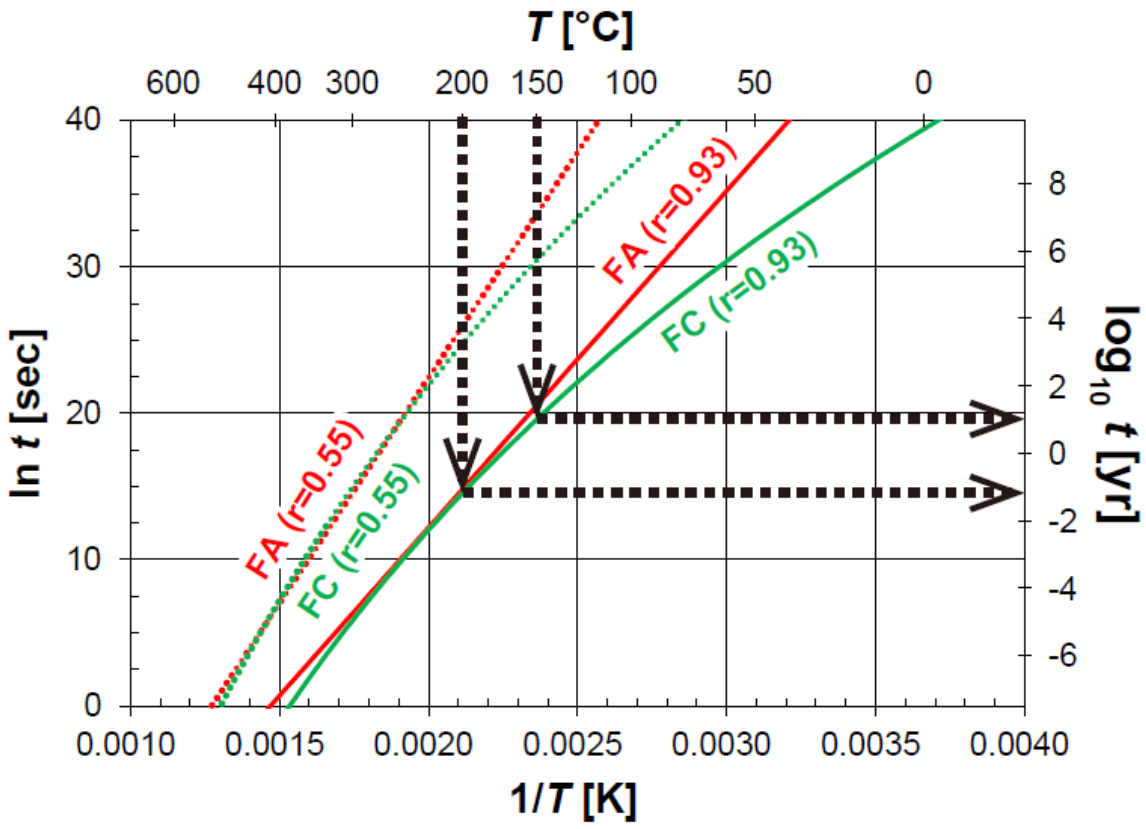

Figure 7. Time–temperature conditions under which AFTs are annealed. Shortening of fission-track lengths is negligible to lower right of $r = 0.93$ curves. Fanning Arrhenius and Fanning curvilinear models were calculated by using Ketcham et al.'s (2007) equations 2, 3, and 6 and fitted parameters from Ketcham et al.'s (2007) Table 5c (obtained from 579 data points from 26 apatites). Effects of Cl contents on annealing kinetics were calibrated according to Ketcham et al.'s (2007) equation 10 and Figure 6a using a Cl content of 0.706 wt% (value at center of all apatite grains from 13 samples used for fission-track analyses). Reduced length value $r = 0.93$ reflects expected low-temperature annealing under surface conditions over geological time scales. Arrows indicate estimated fluid-flow durations (cf. Fig. 2). [AFT, apatite fission track; FA, Fanning Arrhenius model; FC, Fanning curvilinear model; *r*, reduced fission-track length; *t*, time; *T*, temperature]

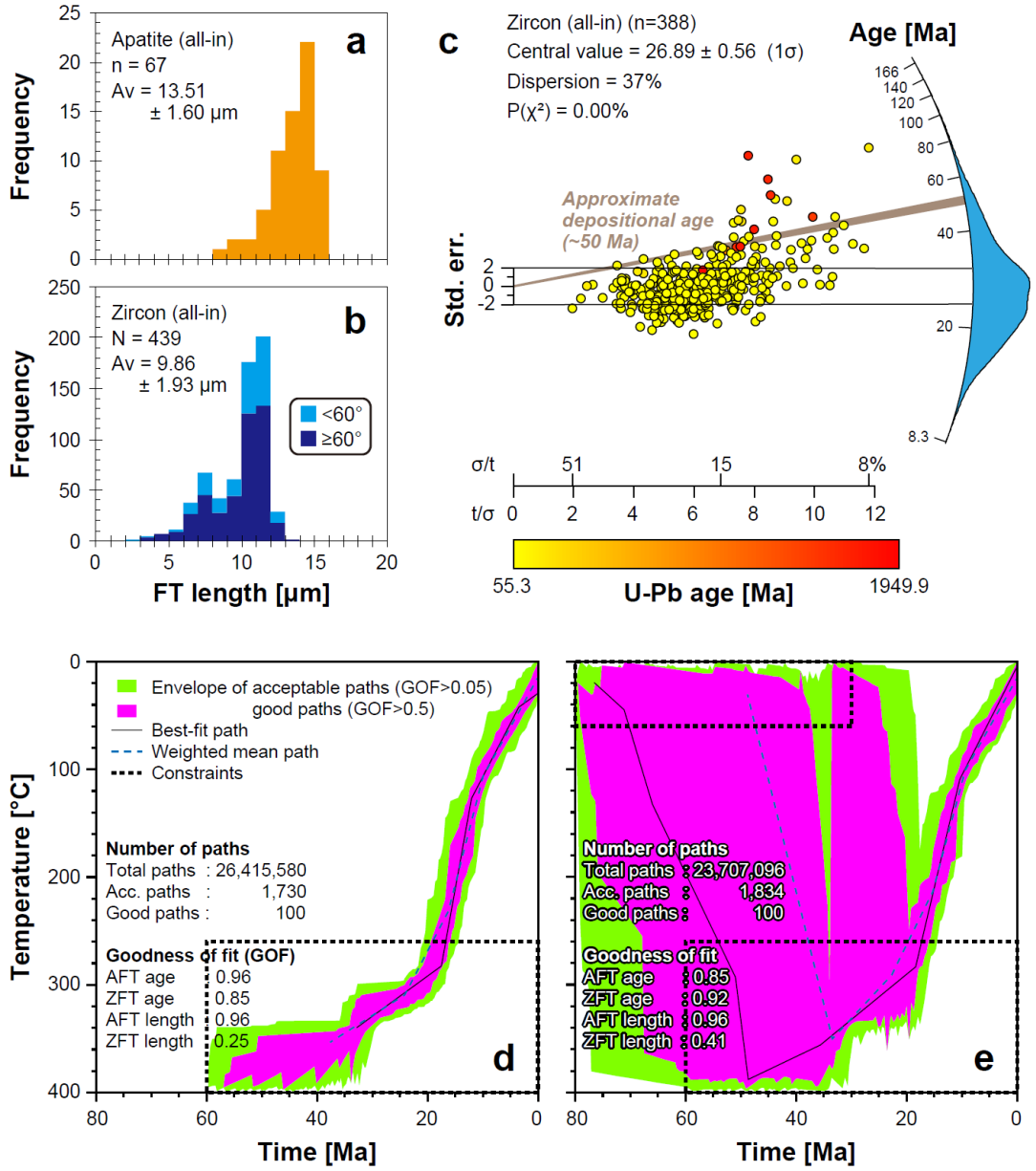

Figure 8. Fission-track length histograms of (a) apatite and (b) zircon, integrated for all 13 samples studied (Supp. Figs. S4 and S5). Track-length distribution of zircon is shown with different fill colors for tracks marking azimuth angles that are higher (dark-blue column) and lower (light-blue column) than 60° to crystallographic *c*-axis, because track lengths in zircon are dependent on etching and annealing properties, which exhibit angular variation (Hasebe et al., 1994; Yamada et al., 1995). (c) Radial plots (Galbraith, 1990) of ZFT ages integrated for all 13 samples. Plots were drawn using RadialPlotter software (Vermeesch, 2009). (d, e) Monotonic-cooling and reheating scenarios. Inverse-thermal-history models based on integrated fission-track ages and track length data; modeling was carried out using HeFTy v.1.9.3 software (Ketcham, 2005). (Supp. Text S4). [Acc., acceptable; AFT, apatite fission track; Av, mean length ±1σ; FT, fission-track; GOF, goodness of fit; *n*, population size; N, number of fission-track lengths measured; ZFT, zircon fission track]

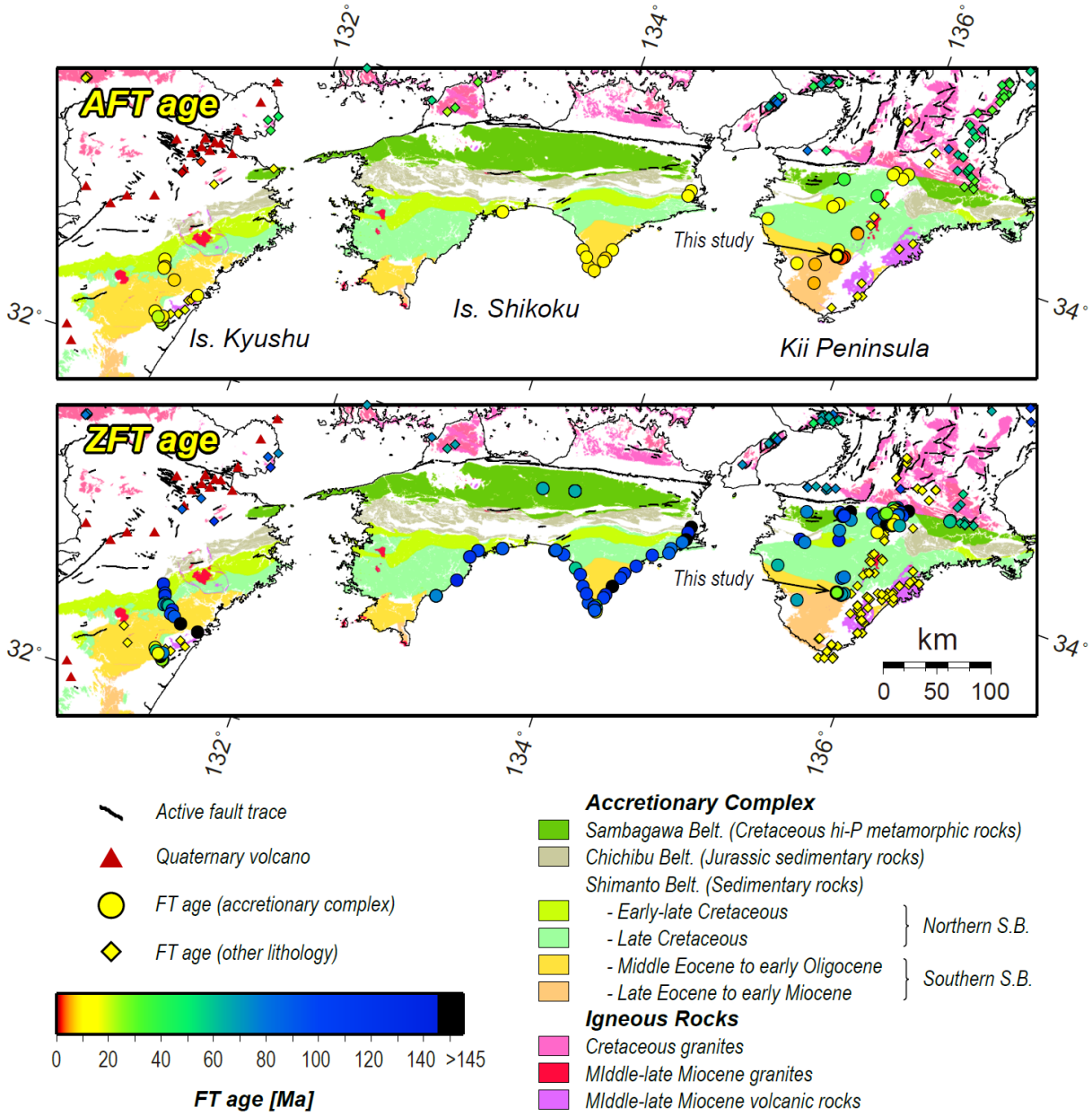

Figure 9. Fission-track ages in Shimanto Belt on forearc side of Southwest Japan Arc. Age data are from low-temperature thermochronological database v.1.05.00 (Sueoka and Tagami, 2019) and references therein. Weighted-mean ages of all 13 samples obtained for this study are plotted at location HJG1 on map. Geologic map is modified after Wakita et al. (2009). Active fault traces and Quaternary volcanoes are from Nakata and Imaizumi (2002) and Committee for Catalog of Quaternary Volcanoes in Japan (1999). [AFT, apatite fission track; FT, fission-track; hi-P, high-pressure; S.B., Shimanto Belt; ZFT, zircon fission track]

Table 1. List of samples.

Sample code	Lithology	L [m]	Corr. L [m]	Analysis performed			
				Fluid inclusion	U-Pb	FT	(U-Th)/He
Loc. HJG1 (N33°49'52.64", E135°43'26.47")							
HJG1-F	Qtz vein	-	-	Y	-	-	-
HJG1-0m	Sandstone	0.0	0.0	-	Y	Y	Y
HJG1-1m	Sandstone	1.1	0.4	-	Y	Y	Y
HJG1-3m	Sandstone	3.1	1.0	-	Y	Y	Y
HJG1-10m	Sandstone	9.9	3.3	-	Y	Y	Y
HJG1-20m	Sandstone	17.1	5.6	-	Y	Y	Y
Loc. HJG2 (N33°49'56.04", E135°43'23.75")							
HJG2-F	Qtz vein	-		Y	-	-	-
HJG2-0m	Sandstone	0.0	0.0	-	Y	Y	Y
HJG2-1m	Sandstone	0.7	0.7	-	Y	Y	Y
HJG2-3m	Sandstone	2.3	2.3	-	Y	Y	Y
HJG2-10m	Sandstone	10.2	10.1	-	Y	Y	Y
Loc. HJG3 (N33°50'02.84", E135°43'18.79")							
HJG3-Upb	Qtz porphyry	-	-	-	Y	-	-
Loc. HJG4 (N33°50'10.26", E135°43'15.27")							
HJG4-F	Qtz vein	-	-	Y	-	-	-
HJG4-0m	Sandstone	0.0	0.0	-	Y	Y	-
HJG4-1m	Sandstone	1.2	1.2	-	Y	Y	-
HJG4-3m	Sandstone	4.2	4.2	-	Y	Y	-
HJG4-10m	Sandstone	11.7	11.6	-	Y	Y	-

Table 1. List of samples. Latitude and longitude of sample localities were obtained by handheld GPS and are shown in WGS84. L indicates horizontal distance from alteration zone along outcrop surfaces, whereas Corr. L denotes horizontal distance from veins calibrated against strikes/dips of alteration zones and strikes of outcrop walls (Fig. 3). [FT, fission-track; Loc., locality; Qtz, quartz; Y, yes (analysis performed on sample)]

Table2. Summary of fluid-inclusion data.

Inclusion No.	Mineral	Inclusion type	T_h [°C]	T_f [°C]	Salt conc. [wt% NaCl]	Note
HJG1-F						
1-1	Qtz	I	**145**	-	-	
1-2	Qtz	II	140	-	-	
1-3	Qtz	II	-	-	-	T_h and T_f were not obtained
1-4	Qtz	II	-	-	-	T_h and T_f were not obtained
1-5	Qtz	II	-	-	-	T_h and T_f were not obtained
1-6	Qtz	II	-	-	-	T_h and T_f were not obtained
1-7	Qtz	II	-	-	-	T_h and T_f were not obtained
1-8	Qtz	II	-	-	-	T_h and T_f were not obtained
1-9	Qtz	II	-	-	-	T_h and T_f were not obtained
1-10	Qtz	I	**144**	-	-	
HJG2-F						
2-1	Qtz	II	186	-1.0	1.7	
2-2	Qtz	II	-	-	-	T_h = 62°C but not reproducible
2-3	Qtz	II	-	-	-	T_h = 104°C but not reproducible
2-4	Qtz	II	-	-	-	T_h = 132°C but not reproducible
2-5	Qtz	II	117	-	-	
2-6	Qtz	II	214	-	-	
2-7	Qtz	II	173	-	-	
2-8	Qtz	II	173	-0.4	0.7	
2-9	Qtz	II	-	-	-	T_h = 118°C but not reproducible
2-10	Qtz	II	-	-	-	T_h = 110°C but not reproducible
2-11	Qtz	I	**195**	**-5.0**	**7.9**	
2-12	Qtz	I	**211**	-	-	
2-13	Qtz	II	187	-5.0	7.9	
2-14	Qtz	II	110	-	-	
2-15	Qtz	II	-	-	-	T_h = 110°C but not reproducible
2-16	Qtz	II	-	-4.5	7.2	
2-17	Qtz	II	216	-2.9	4.8	
HJG4-F			-			
4-1	Qtz	II	-	-	-	monophase liquid inclusion
4-2	Qtz	II	-	-	-	gaseous inclusion
4-3	Qtz	II	-	-	-	gaseous inclusion
4-4	Qtz	II	-	-	-	gaseous inclusion
4-5	Qtz	II	-	-	-	gaseous inclusion
4-6	Qtz	II	-	-	-	gaseous inclusion
4-7	Qtz	II	-	-	-	gaseous inclusion
4-8	Qtz	II	-	-	-	monophase liquid inclusion
4-9	Qtz	II	-	-	-	monophase liquid inclusion
4-10	Qtz	II	-	-	-	monophase liquid inclusion
4-11	Qtz	II	-	-	-	gaseous inclusion
4-12	Qtz	II	-	-	-	gaseous inclusion
4-13	Qtz	II	-	-	-	monophase liquid inclusion
4-14	Qtz	II	-	-	-	monophase liquid inclusion
4-15	Qtz	II	-	-	-	monophase liquid inclusion
4-16	Qtz	I	-	-	-	monophase liquid inclusion

Table 2. Summary of fluid-inclusion data. Inclusion classification based on Roedder's (1984) criteria. [conc., concentration; I, primary inclusion type; II, secondary inclusion type; Qtz, quartz; T_f, final ice-melting temperature; T_h, homogenization temperature, in bold if for primary inclusion]

Table 3. Summary of AFT and ZFT data.

Sample code	grains	Spontaneous FT		U measurement		U standard		U [ppm]	Pooled FT age ± 1σ [Ma]	Cl [wt%]
		ρ_s [10^6 cm^{-2}]	N_s	ρ_U [10^9 cm^{-2}]	N_U	$\rho_{U\text{-std}}$ [10^9 cm^{-2}]	$N_{U\text{-std}}$			
Zircon										
HJG1-0m	28	4.77	1,164	5.59	1,367,571	1.333	15,697	352	26.5 ± 1.2	-
HJG1-1m	30	6.47	1,657	6.35	1,619,317	1.430	16,835	373	34.1 ± 1.4	-
HJG1-3m	30	5.51	1,389	6.08	1,511,646	1.359	16,006	376	29.2 ± 1.3	-
HJG1-10m	30	5.10	1,335	6.15	1,596,112	1.345	15,835	384	26.3 ± 1.1	-
HJG1-20m	30	4.15	1,192	5.13	1,461,429	1.356	15,972	318	25.8 ± 1.2	-
HJG2-0m	30	4.23	1,121	5.55	1,440,745	1.345	15,842	347	24.5 ± 1.1	-
HJG2-1m	30	4.20	1,108	4.55	1,188,763	1.341	15,791	285	29.2 ± 1.4	-
HJG2-3m	30	3.90	1,111	5.02	1,367,704	1.349	15,883	313	25.6 ± 1.2	-
HJG2-10m	30	4.52	1,312	4.62	1,301,212	1.320	15,540	294	31.1 ± 1.4	-
HJG4-0m	30	3.78	993	5.05	1,323,100	1.369	16,116	310	24.0 ± 1.1	-
HJG4-1m	30	4.67	1,229	4.97	1,307,709	1.299	15,299	322	28.5 ± 1.3	-
HJG4-3m	30	5.60	1,293	6.33	1,405,870	1.238	14,581	429	26.6 ± 1.2	-
HJG4-10m	30	5.41	1,559	6.14	1,743,630	1.186	13,967	435	24.8 ± 1.0	-
Apatite										
HJG1-0m	36	0.182	103	0.650	370,749	0.3119	3,820	29	11.0 ± 1.5	0.16
HJG1-1m	36	0.201	164	0.897	718,624	0.3119	3,820	40	9.0 ± 1.0	0.24
HJG1-3m	36	0.187	161	0.736	640,728	0.3119	3,820	33	9.9 ± 1.1	0.15
HJG1-10m	30	0.174	129	0.663	481,343	0.3225	3,951	29	11.0 ± 1.3	0.14
HJG1-20m	30	0.274	194	0.120	824,188	0.3225	3,951	52	9.6 ± 1.0	0.29
HJG2-0m	30	0.359	255	0.118	868,650	0.3225	3,951	51	12.0 ± 1.2	0.31
HJG2-1m	30	0.246	170	0.937	639,748	0.3169	3,883	41	10.7 ± 1.2	0.36
HJG2-3m	30	0.203	132	0.702	430,783	0.3169	3,883	31	12.3 ± 1.5	0.64
HJG2-10m	30	0.187	125	0.820	517,618	0.3169	3,883	36	9.7 ± 1.2	0.33
HJG4-0m	18	0.272	68	0.102	283,953	0.3104	3,803	46	9.4 ± 1.4	0.14
HJG4-1m	30	0.123	82	0.444	272,067	0.3104	3,803	20	11.9 ± 1.7	0.14
HJG4-3m	30	0.202	134	0.793	514,705	0.3104	3,803	36	10.2 ± 1.2	0.71
HJG4-10m	30	0.242	177	0.879	605,794	0.3104	3,803	40	11.5 ± 1.3	0.23

Table 3. Summary of AFT and ZFT data. Apatite chlorine content is correlated to AFT annealing rate (e.g., Carlson et al., 1999). Pooled fission-track ages (t) and their errors (σ) are calculated by equations:

$$t = \frac{1}{\lambda_D} ln\left(1 + \lambda_D \cdot g \cdot \zeta \frac{\sum N_s}{\sum N_U} \rho_{U-std}\right)$$

$$\sigma = t\sqrt{\frac{1}{\sum N_s} + \frac{1}{\sum N_U} + \frac{1}{\sum N_{U-std}} + \left(\frac{\sigma_\zeta}{\zeta}\right)^2}$$

where λ_D is total decay constant of ^{238}U (= 1.55125×10^{-10} yr^{-1}), and g is geometry factor (= 0.5 for internal surfaces). ζ values and their errors (σ_ζ) are 46.8 ± 1.0 for zircon and 254 ± 18 for apatite. Nancy 91500 zircon and Durango apatite were used as uranium standards (Supp. Text S2). [AFT, apatite fission-track; Cl, chlorine content; FT, fission-track; N_s, number of spontaneous tracks; N_U, number of uranium measurements on unknowns; $N_{U\text{-std}}$, number of uranium measurements on standard; ρ_s, density of spontaneous tracks; ρ_U, density of uranium measurements on unknowns; $\rho_{U\text{-std}}$, density of uranium measurements on standard; t, pooled fission-track ages; U, uranium content; ZFT, zircon fission-track]

Table 4. Summary of zircon (U-Th)/He data.

Sample code	Grain ID	Mass [μm]	^{238}U [ppm]	^{232}Th [ppm]	Th/U	^{4}He [ncc/mg]	F_T	eU [ppm]	(U-Th)/He age ± 1σ [Ma] Raw	Corr.	
Unknown							***Weighted mean age ± 1σ:***			***16.8 ± 3.9***	
HJG1-0m	008	2.8	-	-	-	1665.3	-	-	-	-	*
	015	1.3	302.0	162.7	0.54	477.4	0.60	340.3	11.5	19.3 ± 2.2	
HJG1-1m	010	2.8	481.2	242.7	0.50	827.8	0.71	538.2	12.6	17.8 ± 2.0	
	003	2.4	584.4	294.2	0.50	489.0	0.71	653.5	6.2	8.7 ± 1.0	
HJG1-3m	008	2.2	256.8	129.0	0.50	374.1	0.69	287.1	10.7	15.5 ± 1.7	
	004	3.7	570.2	212.8	0.37	910.8	0.75	620.2	12.1	16.2 ± 1.8	
HJG1-10m	009	3.1	901.1	292.4	0.32	1539.6	0.74	969.8	13.0	17.7 ± 2.0	
	013	4.0	605.4	147.6	0.24	585.9	0.73	640.1	7.5	10.3 ± 1.2	
HJG1-20m	006	4.9	312.7	181.5	0.58	652.0	0.75	355.4	15.1	20.2 ± 2.3	
	010	6.2	163.7	68.9	0.42	901.2	0.77	179.8	41.1	53.4 ± 6.0	**
HJG2-0m	002	4.6	147.2	128.0	0.87	210.9	0.76	177.3	9.8	12.8 ± 1.4	
	004	5.7	171.6	110.2	0.64	438.1	0.77	197.5	18.2	23.6 ± 2.6	
HJG2-1m	006	1.9	573.4	372.7	0.65	956.0	0.68	660.9	11.9	17.4 ± 1.9	
	009	1.7	483.1	481.1	1.00	864.2	0.64	596.2	11.9	18.5 ± 2.1	
HJG2-3m	003	5.3	659.8	179.8	0.27	1295.3	0.76	702.0	15.2	20.0 ± 2.2	
	010	2.2	274.5	133.2	0.49	415.8	0.70	305.8	11.2	15.9 ± 1.8	
HJG2-10m	006	3.7	5122.1	12243.4	2.39	635.9	0.73	7999.3	0.7	0.9 ± 0.1	**
	009	3.8	309.1	176.4	0.57	554.9	0.72	350.5	13.0	18.1 ± 2.0	
Fish Canyon Tuff: 28.3 ± 0.4 Ma (ZHe age ± 1σ; Gleadow et al., 20 15)							***Weighted mean age ± 1σ:***			***27.7 ± 3.1***	
FCT3	013	5.1	356.9	213.0	0.60	978.0	0.80	406.9	19.7	24.5	
	015	10.2	202.4	100.9	0.50	870.4	0.80	226.1	31.6	39.5	**
	016	6.1	22.4	20.5	0.92	1211.5	0.78	27.2	356.2	456.2	**
	017	9.2	28.2	197.4	6.99	616.7	0.78	74.6	67.6	87.2	**
	103	9.8	356.9	213.0	0.60	1106.5	0.80	406.9	22.3	27.8	
	108	4.5	342.0	182.1	0.53	1066.0	0.74	384.8	22.7	30.7	

Table 4. Summary of zircon (U–Th)/He data. [a]F_T is α-ejection correlation (Farley et al., 1996; Hourigan et al. (2005). Proxy for alpha-radiation activity is computed as eU = [U] + 0.235[Th] (Shuster et al., 2006). [*, sample lost during U–Th measurement; **, not included in weighted mean calculations; Corr., corrected; eU, effective uranium concentration; ZHe, zircon (U–Th)/He]